Bioorganic Chemistry 164 (2025) 108855

Contents lists available at ScienceDirect

Bioorganic Chemistry

journal homepage: www.elsevier.com/locate/bioorg

8-Amino-1,2,4-triazolo[4,3-*a*]pyrazin-3-one derivatives hybridized with antioxidants: new highly potent and selective human A_{2A} adenosine receptor antagonists as useful agents against cerebral ischemia

Sara Calenda [a], Costanza Ceni [a], Daniela Catarzi [a], Flavia Varano [a], Giulia Vagnoni [a], Gian Luca Bartolucci [a], Marta Menicatti [a], Gabriella Marucci [b], Michela Buccioni [b], Diego Dal Ben [b], Rosaria Volpini [b], Antonella Capperucci [c], Damiano Tanini [c], Martina Venturini [d], Elisa Landucci [e], Clara Santalmasi [d], Federica Cherchi [d], Costanza Mazzantini [e], Anna Maria Pugliese [d], Domenico E. Pellegrini-Giampietro [e], Vittoria Colotta [a,*]

[a] *Dipartimento di Neuroscienze, Psicologia, Area del Farmaco e Salute del Bambino, Sezione di Farmaceutica e Nutraceutica, Università degli Studi di Firenze, Via Ugo Schiff, 6, 50019 Sesto Fiorentino, Italy*
[b] *Scuola di Scienze del Farmaco e dei Prodotti della Salute, Università degli Studi di Camerino, via S. Agostino 1, 62032 Camerino, (MC), Italy*
[c] *Dipartimento di Chimica Ugo Schiff, Università degli Studi di Firenze, via della Lastruccia 3, 50019 Sesto Fiorentino, Italy*
[d] *Dipartimento di Neuroscienze, Psicologia, Area del Farmaco e Salute del Bambino, Sezione di Farmacologia e Tossicologia, Università degli Studi di Firenze, Viale Pieraccini 6, 50139 Firenze, Italy*
[e] *Dipartimento di Scienze della Salute, Sezione di Farmacologia Clinica e Oncologia, Università degli Studi di Firenze, Viale Pieraccini 6, 50139 Firenze, Italy*

A R T I C L E I N F O

Keywords:
A_{2A} adenosine receptor antagonists
Edaravone-hybridized 1,2,4-triazolopyrazin-3-ones
Antioxidant-hybridized 1,2,4-triazolopyrazin-3-ones
Antioxidant-hybridized A_{2A} adenosine receptor antagonists
Ligand-adenosine receptor modeling studies

A B S T R A C T

Cerebral ischemia is a complex pathology resulting from the interplay of diverse mechanisms including the massive release of adenosine and the consequent activation of its receptors. Among them, the A_{2A} adenosine receptor (AR) plays a significant role. Much evidence showed that selective A_{2A} AR antagonists reduce excitotoxicity and exert neuroprotective activity in animal models of cerebral ischemia. Oxidative stress contributes to ischemic brain injury; thus, antioxidants have been intensively investigated as neuroprotective against ischemic stroke.

This work focuses on the identification of dual-acting derivatives able to block the A_{2A} AR and exert antioxidant effects because they could be more potent neuroprotective than single-acting compounds. Thus, a set of 8-amino-6-aryl-2-phenyl-1,2,4-triazolo[4,3-*a*]pyrazin-3-ones hybridized with the antioxidant edaravone (EDA) (**1–5**) and (*S*)-2-oxothiazolidine-4-carboxylic acid (OTC) (**6–8**) were synthesized. The new derivatives were potent hA_{2A} AR antagonists (K_i = 1.7–117 nM), endowed with good selectivity versus the other AR subtypes.

Molecular docking studies revealed that these derivatives bind optimally to the A_{2A} AR, with the 2-phenyl ring positioned deep within the receptor cavity and the 6-substituent located near the entrance. Selected compounds, hybridized with EDA and OTC, were effective in reducing neuronal damage caused by oxygen and glucose deprivation in rat hippocampal models of cerebral ischemia. The findings suggested that the neuroprotective effects of EDA-based derivatives **3** and **4** may result from both their antioxidant properties and their ability to antagonize the A_{2A} AR. These results highlighted the therapeutic potential of dual-acting compounds, combining antioxidant activity and A_{2A} AR antagonism, for the treatment of cerebral ischemia and other oxidative stress-related disorders.

Abbreviation: AD, Anoxic depolaritation; AR, Adenosine receptor; d.c, Direct current; DCM, Dichloromethane; DIPEA, Diisopropilethylamine; EDA, Edaravone; EDCI, 1-(3-(dimethylamino)-propyl))-3-ethylcarbodiimide; fEPSP, Field excitatory post sinaptic potential; HOBt, 1-hydroxybenzotriazole; OTC, (*S*)-2-oxothiazolidine-4-carboxylic acid; OGD, Oxygen-glucose deprivation; r.t., Room temperature; TFA, Trifluoroacetic acid.

* Corresponding author.
E-mail address: vittoria.colotta@unifi.it (V. Colotta).

https://doi.org/10.1016/j.bioorg.2025.108855
Received 18 June 2025; Received in revised form 28 July 2025; Accepted 4 August 2025
Available online 6 August 2025

1. Introduction

Adenosine is a key regulator involved in numerous physiological processes, exerting its effects by binding to four types of G protein-coupled receptors: A_1, A_{2A}, A_{2B}, and A_3 adenosine receptors (ARs).

A_1 AR and A_3 AR are coupled to Gi/Go proteins, leading to inhibition of adenylyl cyclase (AC) and a subsequent decrease in intracellular cAMP levels. Additionally, their function varies depending on the specific cell type, as they can influence other signaling pathways.

The A_1 AR is widely expressed in the central nervous system (CNS), particularly in the cortex, cerebellum, hippocampus, spinal cord, and glial cells, where it modulates neurotransmitter release, neural excitability, and induces sedative, anticonvulsant, and anxiolytic effects [1]. Activation of the A_1 AR under ischemic conditions exerts neuroprotective effects by inhibiting glutamate release, and limiting calcium influx, thereby decreasing neuronal damage and promoting cell survival. [2]. A_1 AR is also abundant in peripheral organs, including the heart, kidneys, airways, and immune cells. It induces cardioprotective effects during ischemic stress, it reduces renal function, while stimulates bronchoconstriction, and proinflammatory response [1]. The A_3 AR is expressed at low levels in the brain [3], in regions such as the thalamus, hypothalamus, hippocampus, cortex, and retina, as well as in microglia and astrocytes. Its activation has been shown to provide protection against neurodegeneration and neuroinflammation [1,2]. Peripherally, A_3 AR is found in the coronary and carotid arteries [4], the gastrointestinal tract, lungs, and a wide range of immune and inflammatory cells, where it primarily exerts anti-inflammatory actions [1,2].

A_{2A} and A_{2B} ARs are coupled to Gs proteins, which activate AC and elevate cAMP production, thereby initiating diverse downstream signaling cascades depending on the specific cellular context.

The A_{2A} AR is expressed both in periphery and in the CNS. In the brain, there is the highest density of this AR in the corpus striatum, nucleus accumbens, and olfactory tubercles, and it is also present in the hippocampus and cortex [1]. The A_{2A} AR is expressed in both pre- and post-synaptic neurons, as well as in glial cells, where it promotes pro-inflammatory activity, by driving microglia and astrocytes toward a pro-inflammatory phenotype, particularly under stress conditions such as cerebral ischemia [5]. In peripheral tissues, the A_{2A} AR plays a role in regulating coronary circulation due to its expression in vascular smooth muscle and endothelial cells, where it facilitates vasodilation and contributes to heart-protective effects [6]. The cardioprotective role of this AR is also linked to its ability to limit neutrophil infiltration, a result of its strong anti-inflammatory function [7].

The A_{2B} AR is widely expressed in the bladder, intestine, and fibroblasts, where it plays pro-nociceptive and pro-inflammatory roles. The A_{2B} AR is present at low levels in the CNS, including the spinal cord, where it modulates inflammation and neuronal damage following cerebral ischemia [1]. Recent studies support a neuroprotective role for the A_{2B} AR in ischemic stroke, as demonstrated by the improvement in neurological function and reduction of brain injury observed following administration of a selective A_{2B} AR agonist [8].

As reported above, the A_{2A} AR mediates some of adenosine's effects during stressful conditions, such as those triggered by hypoxia following cerebral ischemia. During hypoxic events, extracellular adenosine levels rise markedly, increasing from nanomolar to micromolar concentrations [9]. Furthermore, there is an upregulation of A_{2A} AR expression in both neurons and microglia, resulting in amplified A_{2A} AR signaling. Research into the involvement of A_{2A} AR in cerebral ischemia has yielded mixed findings, which largely depend on the timing of observation and the specific mechanisms responsible for the injury [10]. Blocking this receptor with antagonists administered within the first hour after ischemia has been found to offer neuroprotective effects [10]. Specifically, antagonism of the A_{2A} AR in neurons results in decreased glutamate release, a process that is significantly upregulated during stroke, and enhances GABAergic signaling, both of which contribute to neuroprotection. Supporting the detrimental role of A_{2A} AR, studies have shown that knockout mice lacking this receptor exhibited smaller infarct areas after focal cerebral ischemia when compared to their wild-type counterparts [10]. Additionally, mice lacking A_{2A} AR expression in the endothelium showed reduced infarct size 24 h post-stroke [11]. Further, inhibition of the A_{2A} AR has been reported to suppress the activation of ERK1/2 MAP kinases, thereby limiting microglial activation and reducing the subsequent release of pro-inflammatory cytokines [12].

Cerebral ischemia and the following reperfusion lead to mitochondrial dysfunction and oxidative stress, with enhanced ROS production which leads to neuronal death, due to oxidation of key cellular components, such as DNA, lipids, and proteins [13,14]. On this basis, antioxidants have been investigated for their potential protective effects against ischemic stroke [14], with some demonstrating neuroprotective properties in experimental models. Given the multifactorial nature of ischemia-induced damage, recent research has increasingly focused on identifying multitarget therapies for ischemic stroke aiming to modulate oxidative pathways alongside other pathological mechanisms [13,15,16].

In this scenario, we planned the synthesis of dual-acting agents capable of blocking the A_{2A} AR and exerting antioxidant effects as they might offer greater neuroprotective potential than single-acting compounds (Fig. 1).

In a previous paper, we described a set of antioxidant-conjugated 8-amino-1,2,4-triazolo[4,3-*a*]pyrazin-3-one derivatives some of which demonstrated high potency and selectivity as hA_{2A} AR antagonists [17]. These compounds featured a phenol or lipoic acid as the antioxidant portion attached at the 6-position of the heteroaromatic core. Herein, we describe a new set of 1,2,4-triazolo[4,3-*a*]pyrazin-3-ones hybridized with the antioxidant edaravone (EDA) and (*S*)-2-oxothiazolidine-4-carboxylic acid (OTC) (Fig. 2, derivatives **1–8**).

EDA, namely 3-methyl-1-phenyl-1H-pyrazol-5(4H)-one, is a drug marketed in Japan for the treatment of acute cerebral ischemia [18]. It protects against neuronal damage but its mechanism of action remains not completely understood. Much evidence showed that the protective effect of EDA is due, but not limited, to its free radical scavenging ability [19]. EDA reduced early accumulation of lipid peroxidation products and oxidative DNA damage and exerted anti-inflammatory effects resulting in a reduction of inducible NO synthase production [20]. In other studies, EDA decreased injury of vascular endothelial cells and the related ischemic cerebral edema and ameliorated neurological function [21,22].

OTC is a pro-drug of *L*-cysteine, into which it is transformed by the ubiquitous intracellular enzyme 5-oxoprolinase [23]. OTC proved to be effective in repleting intracellular stores of glutathione (GSH), and enhancing GSH/GSSG ratio. OTC proved to work as an antioxidant [24,25], and to decrease cell damage and neuroinflammation induced by oxidative stress in several cellular and animal models [23–27]. OTC reduced neuronal death induced, in vitro and in vivo, respectively by oxygen and glucose deprivation (OGD) and by reperfusion injury [26]. Due to these properties, we chose OTC to hybridize our triazolopyrazine series of A_{2A} AR antagonists, with the idea that the attached OTC ring inside the cell might be opened by the intracellular 5-oxoprolinase, unmasking the cysteine residue that could elicit an antioxidant effect [28].

EDA and OTC were connected to the para-position of the 6-phenyl ring using linkers that varied in length and flexibility, potentially influencing the molecule's fit and interaction with the target receptor. The position of the conjunction was chosen based on previous studies suggesting that bulky groups in this position not only maintain high A_{2A} AR affinity but may also enhance A_{2A} AR selectivity. Molecular docking studies showed [17] that these ligands were arranged in the binding cleft with the 2-phenyl group located in the depth of the cavity and the 6-bulky substituent pointing toward the extracellular environment, thus not hindering receptor-ligand interaction.

Some of the newly synthesized compounds, both EDA- and OTC-hybrids (**3**, **4** and **6**, **8**), were selected for their affinity and selectivity

toward the hA_{2A} adenosine receptor and evaluated in in vitro models of cerebral ischemia.

2. Results and discussion

2.1. Chemistry

Derivatives **1–8** were synthesized as depicted in Schemes 1–4. EDA-containing triazolopyrazines **1** and **2** (Scheme 1) were obtained starting from the amino-substituted derivatives **9** [29] and **10** [27] which were transformed into compounds **11** and **12**, respectively, by reaction with *N*-Boc-protected 4-hydrazinobenzoic acid [30], in anhydrous DMF and the presence of 1-(3-(dimethylamino)-propyl))-3-ethylcarbodiimide (EDCI) hydrochloride, 1-hydroxybenzotriazole (HOBt) and Et_3N.

Derivatives **11** and **12** were treated with trifluoroacetic acid (TFA) to give the corresponding hydrazine derivatives. The hydrazine derivative **13** was isolated, characterized, and then reacted with ethyl acetoacetate to give the EDA-conjugated derivative **1**. Instead, the hydrazine derivative formed by deprotection of the *N*-Boc derivative **12** (not shown) was not isolated but was directly reacted with ethyl acetoacetate to give **2**.

The triazolopyrazine derivatives **3** and its superior homolog **4**, containing only the pyrazolone moiety of EDA, i.e. its antioxidant portion, were synthesized as reported in Scheme 2, i.e. starting from the 6-(4-aminophenyl)-substituted derivative **9** [29] which was reacted with chloroacetic acid and 3-chloropropionic acid, in anhydrous DMF and in the presence of EDCI hydrochloride and HOBt, to give, respectively, the amide derivatives **14** and **15** [17]. These latter were heated at reflux, respectively, with anhydrous hydrazine in absolute EtOH and hydrazine monohydrate in anhydrous THF, to give the related hydrazine derivatives **16** and **17**. Finally, the final triazolopyrazines **3** and **4** were obtained after treatment of **16** and **17** with ethyl acetoacetate in EtOH.

EDA-hybridized triazolopyrazine **5** was prepared as illustrated in Scheme 3. The 6-(4-(2-hydroxyethoxy)-phenyl-substituted triazolopyrazine **18** [31] was converted into the corresponding bromo-derivative **19** through a reaction with *N*-bromosuccinimide and triphenylphosphine, in anhydrous dichloromethane. Treatment of compound **19** with anhydrous hydrazine in absolute EtOH gave the hydrazine-derivative **20** which was cyclized with ethyl acetoacetate to give the EDA-hybridized derivative **5**.

The EDA-hybridized compounds **1–5**, as well as EDA, can exist in the tautomeric forms A, B, and C (Fig. 3) [32,33] whose relative abundance depends on the molecule structure and the polarity of the medium. ^1H

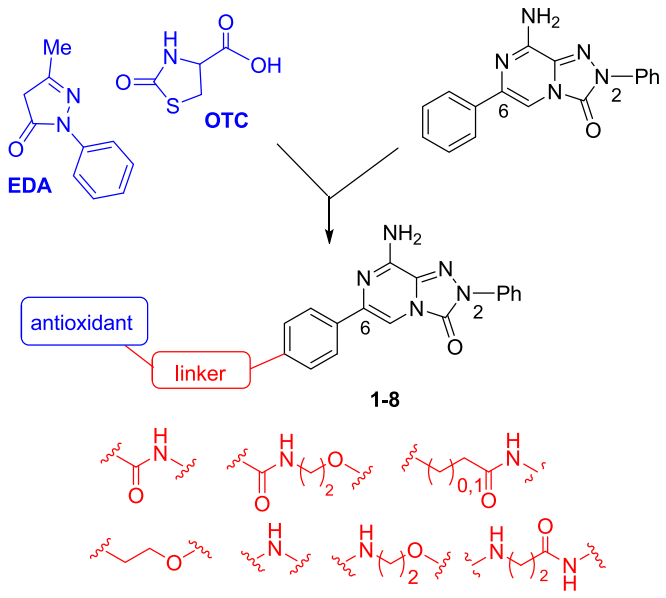

Fig. 2. Hybridization approach to obtain the herein reported antioxidant-based 1,2,4-triazolo[4,3-*a*]pyrazin-3-one derivatives **1–8**.

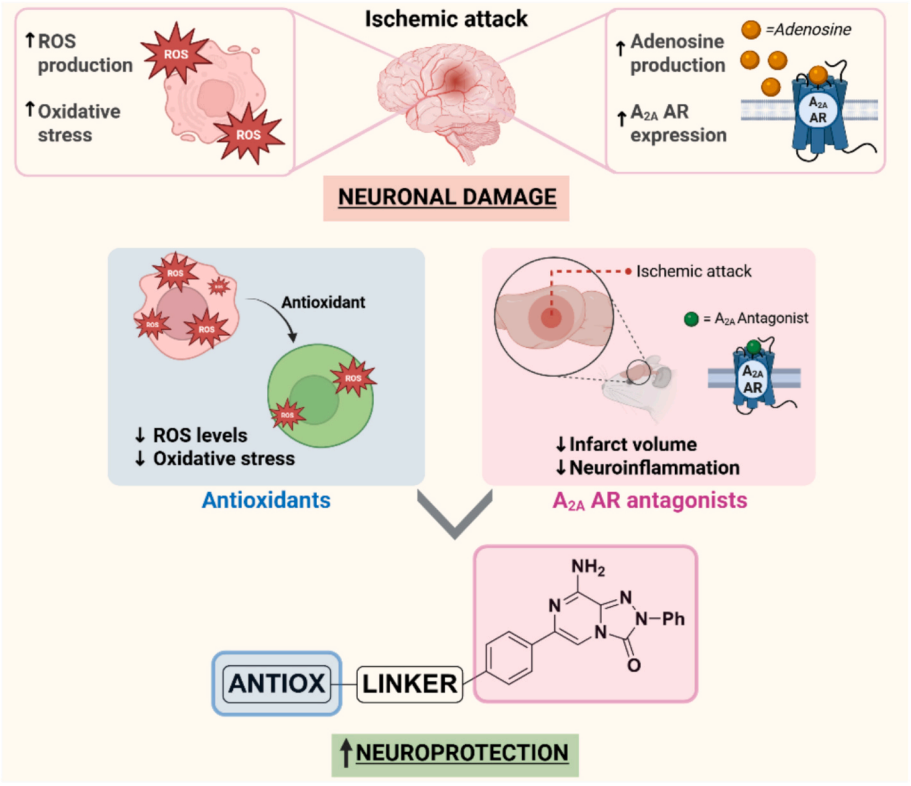

Fig. 1. Rationale for the design and synthesis of dual-acting antioxidant-A_{2A} AR antagonists (Image created using BioRender.com.).

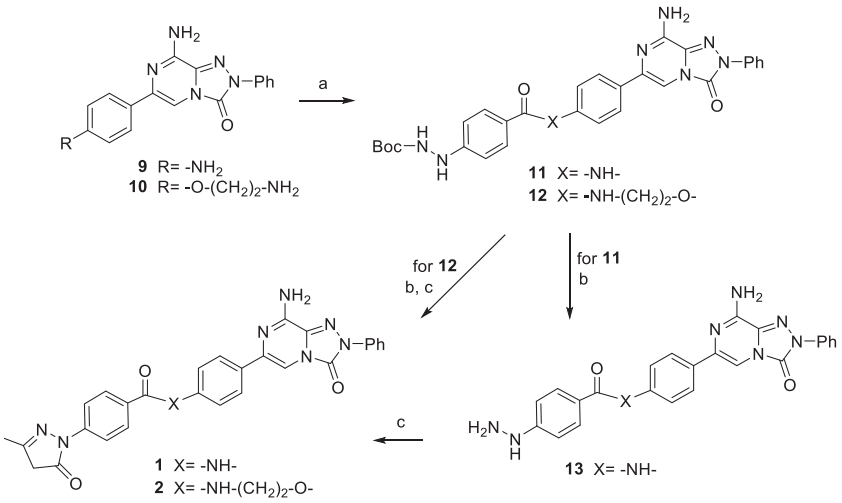

Scheme 1. Reagents and conditions: (a) *N*-Boc-NH-NH-C_6H_4–4-COOH, EDCI hydrochloride, Et_3N, HOBt, anhydrous DMF, from r.t. to 35 °C; (b) TFA, anhydrous DCM; c) ethyl acetoacetate, 60 °C.

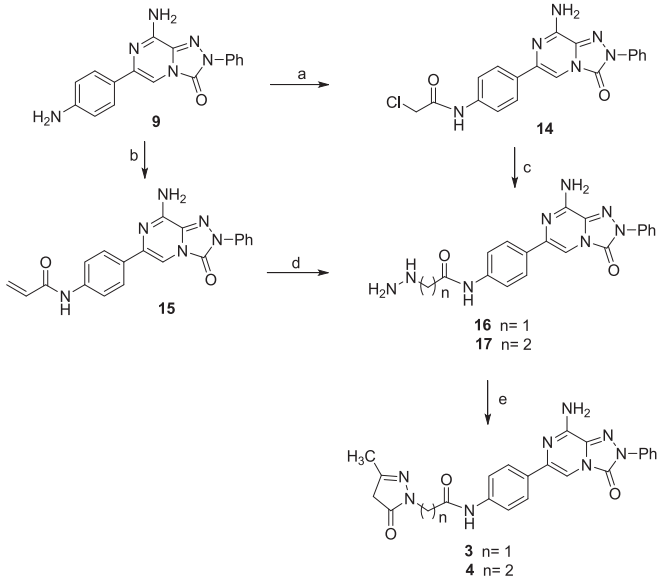

Scheme 2. Reagents and conditions: a) chloroacetic acid, EDCI hydrochloride, HOBt, anhydrous DMF; b) 3-chloropropionic acid, EDCI hydrochloride, DIPEA, anhydrous DMF; c) anhydrous hydrazine, absolute EtOH, reflux; d) hydrazine monohydrate, anhydrous THF, reflux; e) ethyl acetoacetate, EtOH, 60 °C.

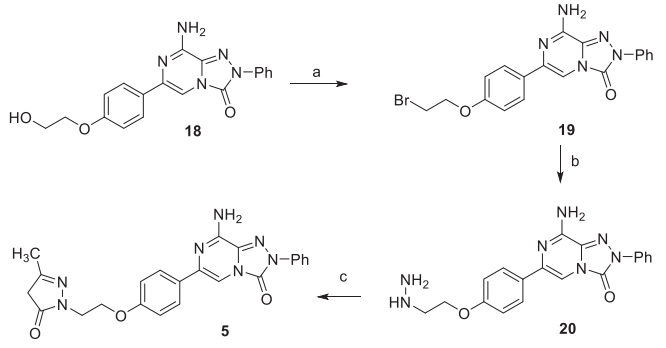

Scheme 3. Reagents and conditions: (a) PPh_3, *N*-bromosuccinimide, anhydrous dichloromethane, from 0 °C to 60 °C; (b) anhydrous hydrazine, EtOH abs, reflux; (c) ethyl acetoacetate, EtOH, 60 °C.

NMR spectra indicated that in $DMSOd_6$ solution, derivatives **1–5** exist as tautomers **A** and/or **B**, the latter being more abundant. In particular, the spectra of compounds **1** and **3** showed two-proton signal at about 3.50 δ attributable to the pyrazole -CH_2- of tautomer **A**, a one-proton singlet at about 5.1–5.4 δ assignable to the H_4 proton of **B**, and a signal at about 10–11 δ attributable to the NH. Tautomer **C** has been excluded because the chemical shift of the H_4 signal (5.1–5.4 δ) is more consistent with an olefinic proton (tautomer **B**) rather than an aromatic proton (tautomer **C**), which should appear at $\delta > 6$ [34]. For simplicity, in figures and schemes, compounds **1–5** are reported in the tautomeric form **A**, and also their chemical names were referred to this tautomer.

The OTC-conjugated triazolopyrazines **6, 7** and **8** (Scheme 4) were obtained by reacting the amino derivatives **9** [29], **21** [17] and **10** [29], respectively, with *(R)* 2-oxothiazolidine-4-carboxylic acid [35], activated by EDCI hydrochloride and HOBt.

2.2. Structure-affinity relationships

The new hybridized triazolopyrazines were tested to measure their affinity and selectivity for the hA_{2A} AR versus the other ARs. The results are reported in Table 1, together with those of the triazolopyrazine **24** [17] which was tested as a reference hA_{2A} antagonist in the in vitro models of cerebral ischemia.

The results aligned with our expectations, as all the new compounds **1–8** exhibited nanomolar affinity for the hA_{2A} AR (K_i values ranging from 1.7 nM to 117 nM) and different degrees of selectivity versus the other hAR subtypes. All compounds resulted to be inactive in the cAMP assays at the hA_{2B} AR ($IC_{50} > 30{,}000$ nM). Derivatives showing the best affinity at the hA_{2A} AR were the OTC-conjugated compounds **8** ($K_i = 1.7$ nM) and **6** ($K_i = 8.1$ nM) which showed also high selectivity vs hA_1 and hA_3 ARs. Instead, the OTC-derivative 7 was the least active at the hA_{2A} AR, among the herein reported derivatives ($K_i = 117$ nM). The significantly lower hA_{2A} AR affinity of compound **7**, compared to compounds **6** and **8**, could be due to the longer linker between the OTC-moiety and the 6-phenyl ring, which may reduce key receptor–ligand interactions. The EDA-conjugated triazolopyrazines **1**, **2** showed similar hA_{2A} AR binding activities and comparable selectivity profiles. Specifically, they did not bind the hA_1 AR, while both exhibited hA_3 AR affinity in the high nanomolar range ($K_i = 512$ nM and 324 nM, respectively). These results indicate that the diversity of the linker between EDA moiety and the 6-phenyl ring did not affect a lot the ligand-receptor interactions. This finding is further supported by compounds **3–5**, which contain only the pyrazole ring of EDA, known to be responsible for the antioxidant activity. These derivatives exhibited hA_{2A} AR affinity comparable to that

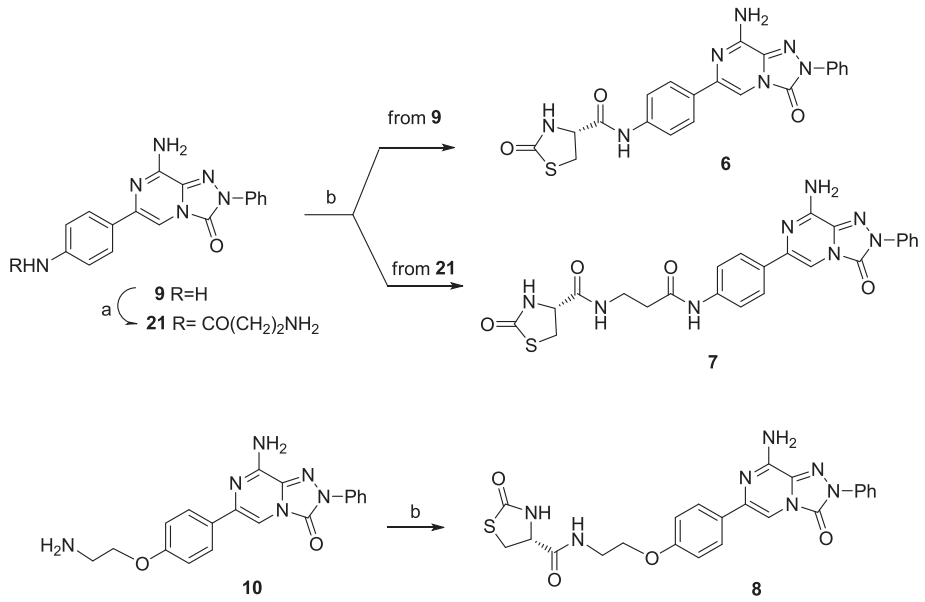

Scheme 4. Reagents and conditions: a) see Ref. 17; b) (*R*) 2-oxothiazolidine-4-carboxylic acid, EDCI hydrochloride, DIPEA, HOBt, anhydrous DMF, r.t.

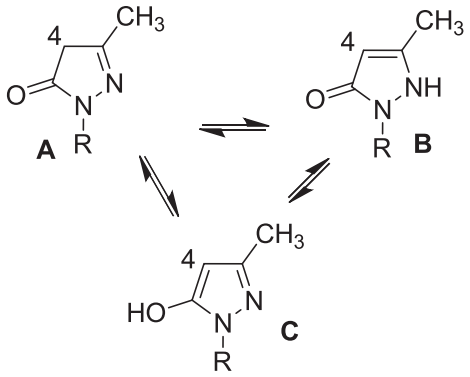

Fig. 3. Tautomeric forms of EDA-based derivatives **1–5**.

of compounds **1** and **2**, with the most potent being compounds **3** (K_i = 57 nM) and **5** (K_i = 69 nM). The latter also showed hA_3 AR affinity in the high nanomolar range (K_i = 358 nM and 128 nM, respectively), while they were inactive at the hA_1 AR. To rationalize the observed affinity and selectivity data, docking studies were carried out at ARs (see paragraph 2.5).

EDA-hybridized derivatives **3** and **4** and the OTC derivatives **6** and **8** were selected for their high hA_{2A} AR affinity and selectivity versus the hA_1 AR (**3, 6, 8**) or hA_3 AR (**4, 6, 8**) to be pharmacologically profiled in in vitro models of cerebral ischemia. Thus, cAMP assays in hA_{2A} AR-CHO cells were carried, and the antagonistic activity of compounds **3, 4, 6,** and **8** was confirmed, as they were able to inhibit NECA-stimulated adenylyl cyclase activity at nanomolar concentration (Table 2).

It has to be noted that selectivity versus the A_1 AR is a critical feature of potential drugs against ischemic stroke, as blocking A_1 AR would remove its inhibitory control, leading to increased glutamate release, enhanced excitotoxicity, and greater neuronal injury [1,2]. In addition, A_3 AR blockade may also be harmful, as recent studies have highlighted the neuroprotective role for this AR subtype in animal models of cerebral ischemia [2]. Moreover, selectivity versus A_1 and A_3 ARs is important for cardiovascular safety, especially in stroke patients. Antagonizing A_1 AR may disrupt heart rate control and conduction, increasing risks of tachycardia or arrhythmias, while A_3 antagonism might interfere with protective anti-inflammatory and vasodilatory effects. Therefore, high selectivity for the A_{2A} AR helps minimize potential cardiovascular side effects in these patients [1,2].

2.3. Antioxidant activity of EDA-hybridized compounds *3* and *4*

The free-radical scavenging activity of compounds **3** and **4**, selected for further pharmacological tests, was evaluated by the 2,2-diphenyl-1-picrylhydrazyl (DPPH) assay, following a slightly modified previously described procedure [36]. OTC-conjugated derivatives **6–8** were not evaluated because OTC, per se, is not a free-radical scavenger, thus being inactive in the DDPH assay [37].

DPPH is a purple stable free radical that in the presence of a hydrogen atom-donating compound turns into the yellow non-radical form. This transformation can be measured spectrophotometrically. The absorption of DPPH at 517 nm was observed to decrease in the presence of the tested compounds, with a linear increase in the consumption of the radical DPPH. Radical scavenging activity (%) was reported as the percentage of DPPH discoloration and the values were plotted into a graph showing the average inhibition of DPPH radical at the steady-state as a function of the compound concentration (Fig. 4). Ascorbic acid and EDA were used as reference antioxidants, while compound **24**, possessing no antioxidant portion, was the negative control. The EC_{50} values, defined as the compound concentrations required to reduce the DPPH concentration by 50 %, are reported in Table 3.

Interestingly, the EDA-hybridized compounds **3** and **4** showed good radical scavenging ability, higher than that of EDA.

2.4. Chemical stability

The EDA-hybridized compounds **3** and **4** along with the OTC-conjugated derivatives **6** and **8,** contain functionalities that might be somewhat labile. Therefore, we considered it important to investigate their stability in a 50 mM Tris(hydroxymethyl)aminomethane hydrochloride buffer (50 mM Tris buffer, pH = 7.4, see paragraph 4.3). Degradation profiles were obtained by plotting the natural logarithm of analyte concentration versus incubation time (Fig. S1–S4, Supplementary Data), revealing that all compounds remained stable under these conditions. Further investigations will focus on evaluating the stability of these derivatives in human plasma, which is a fundamental prerequisite for exploring their pharmacokinetic profile and progressing toward in vivo evaluation.

Table 1
Binding and functional activity at human adenosine receptors[a].

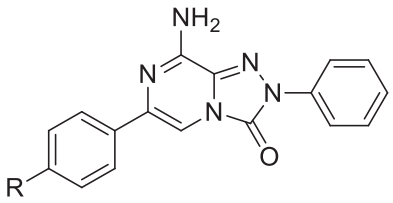

		Binding experiments K_i (nM)			cAMP assays IC_{50} (nM)
	R	hA_1[b]	hA_{2A}[c]	hA_3[d]	hA_{2B}[e]
1	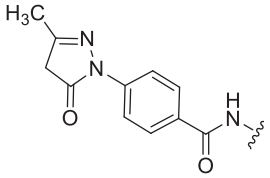	>30,000	75 ± 18	512 ± 110	>30,000
2	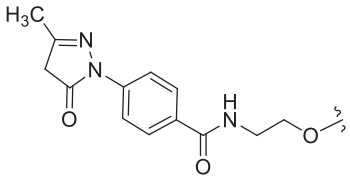	>30,000	85 ± 24	324 ± 63	>30,000
3	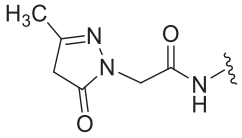	>30,000	57 ± 11	358 ± 5	>30,000
4	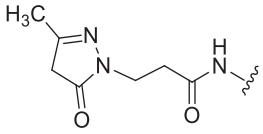	581 ± 40	91 ± 8.5	>30,000	>30,000
5	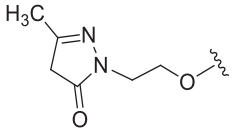	>30,000	69 ± 12	128 ± 19	>30,000
6	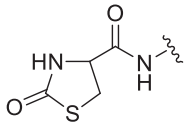	504 ± 129	8.1 ± 0.83	1140 ± 167	>30,000
7	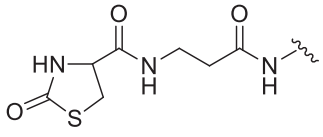	371 ± 17	117 ± 18	4686 ± 11	>30,000
8	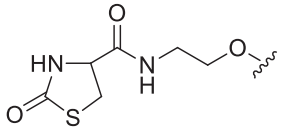	173.4 ± 37	1.7 ± 0.36	868 ± 169	>30,000
24[f]	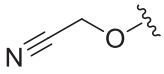	> 30,000	8.2 ± 2.3	> 30,000	> 30,000

[a] Data (n = 3–5) are expressed as means ± standard errors.
[b] Displacement of specific [^{3}H]-CCPA binding at hA_1 AR expressed in CHO cells.
[c] Displacement of specific [^{3}H]-NECA binding at hA_{2A} AR expressed in CHO cells.
[d] Displacement of specific [^{3}H]-HEMADO binding at hA_3 AR expressed in CHO cells.

[e] IC_{50} values of the inhibition of NECA-stimulated adenylyl cyclase activity in CHO cells expressing hA_{2B} AR.
[f] Reference [17].

Table 2
Potencies of the selected triazolopyrazines **3, 4, 6** and **8** at hA_{2A} AR.

	hA_{2A} AR [a](IC_{50} nM)
3	1416 ± 125
4	1863 ± 217
6	403 ± 77
8	118 ± 21
24[b]	157 ± 43

[a] IC_{50} values of the inhibition of NECA-stimulated adenylyl cyclase activity in CHO cells expressing hA_{2A} AR. Data are expressed as means ± standard errors.
[b] Reference 17.

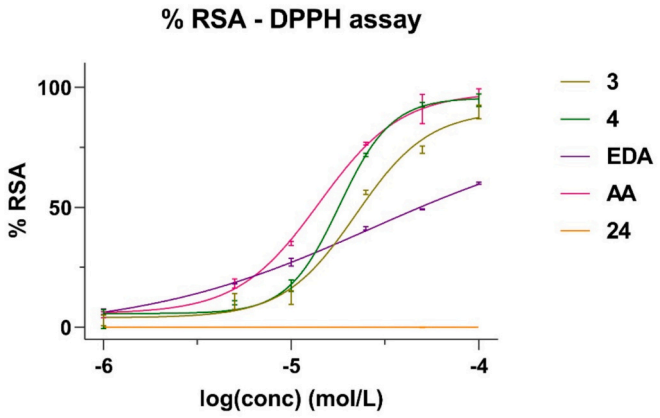

Fig. 4. Radical scavenging activity (RSA) of compounds **3** and **4**. EDA and ascorbic acid (AA) were used as reference antioxidants, and compound **24** as the negative control.

Table 3
EC_{50} values are compound concentrations causing a 50 % decrease in the DPPH absorbance.

	EC_{50} (μM)
3	22.21 ± 0.59
4	18.09 ± 0.36
EDA	26.61 ± 1.33
AA[a]	14.15 ± 1.30
24	*Inactive*

Values are mean ± SD, $n = 3$.
[a] Ascorbic acid.

2.5. Molecular modeling studies

Docking studies with the novel compounds were performed at the binding cavity of the antagonist-bound hA_{2A} AR (pdb code: 5NM4 [38]). MOE (Molecular Operating Environment 2022.02) modeling suite [39] docking tool and CCDC Gold software [40] were used in this task. Additional experiments were carried out to analyze the selectivity of the novel compounds, by performing docking experiments at 3D structures of hA_1 AR (pdb code: 5N2S [41]) and hA_3 AR (pdb code: 8X16 [42]), with the same protocols.

The most frequent, and highest score-associated, binding mode of the analyzed molecules at the hA_{2A} AR structure presents the core scaffold placed in the center of the receptor cavity (Fig. 5), making interactions with residues Phe168, belonging to the extracellular loop (EL) 2 segment, and Leu249$^{6.51}$.

The 2-phenyl ring points toward the most internal part of the binding cavity, getting in proximity to residues Val84$^{3.32}$, Leu85$^{3.33}$, Trp243$^{6.48}$, His250$^{6.50}$, and Leu249$^{6.51}$. The amino group in the 8-position makes H-bonds with Asn253$^{6.55}$ and Glu169 (EL2) residues, in analogy with several ligands co-crystallized with the hA_{2A} AR. The large 6-substituent is headed toward the extracellular space, getting in proximity to TM1, TM2, and TM7 (i.e. Ile66$^{2.64}$, Met270$^{7.35}$, Tyr271$^{7.36}$, and Ile274$^{7.39}$) and EL2 and EL3 segments (i.e. Lys153, Phe168, and His264) residues, making polar or non-polar interactions with these amino acids. The para-amide group in the 6-phenyl ring (compounds **1**, **3**, **4**, **6**, **7**) may give polar interactions with the backbone carbonyl oxygen of Ile66$^{2.64}$ and/or with the para-hydroxyl group of the Tyr271$^{7.36}$ side chain (see docking conformation of compound **3** at the hA_{2A} AR, Fig. 5). The length of the linker between the 6-phenyl group and the 1H-pyrazol-3(2H)-one moiety of EDA makes this last group being located in various positions at the most external region of the receptor, with potential interactions with Ser67$^{2.65}$, Thr68$^{2.66}$, Lys153 (EL2), Leu167 (EL2), Leu267$^{7.32}$, and Tyr271$^{7.36}$ residues (Fig. 5).

Since NMR analyses suggested that the pyrazol-3-one group might be present as more than one tautomer, we simulated the potential interaction of compound **3** in the hA_{2A} AR cavity with the presence of various tautomers of this ring. The results are shown in Fig. 5 (C-E). Two of these tautomers present an H-bond donor function that may interact with the above-cited residues in the TM2 domain (i.e. Ser67$^{2.65}$ or Thr68$^{2.66}$). One of these tautomer (tautomer A, Fig. 3) lacks the H-bond donor and cannot interact with these residues. For all these tautomers is still possible a polar interaction with the EL2 residue Lys153.

Compounds presenting a different linker (**4**–**5**) are still able to make polar interactions with residues present in the TM2, EL2, and TM7 domains of the hA_{2A} AR, even if with lower affinity compared to **3**. The linker of compound **5** is of the same length of the one present in compound **3**, even if lacking the amide function. Docking results show that its pyrazol-3-one ring is still able to make polar interaction with EL2 residue Lys153 and/or TM2 residues (i.e. Ser67$^{2.65}$ or Thr68$^{2.66}$). On the other hand, the linker of compound **4** presents the same amide function of **3** and analogue interaction with the Ile66$^{2.64}$ residue, but the longer length of the linker appears to prevent the pyrazol-3-one group to make a stable polar interaction with the receptor (the comparison of the docking suggested interaction of compounds **3**–**5** with the hA_{2A} AR is reported in Fig. S6, Supplementary Data).

Results of docking simulations suggest that the compounds bearing an OTC moiety adopt a similar arrangement within the binding site compared to the EDA-bearing ones, making also analogue interaction with the binding cavity. Even in this case, the size of the spacer between the 6-phenyl group and the terminal cyclic moiety makes this last function being located in various positions at the external region of the receptor cavity, close to the side chains of Ser67$^{2.65}$, Lys153 (EL2), Leu167 (EL2), and Leu267$^{7.32}$ residues (see docking conformation of compound **8** in Fig. 6). As observed for compounds **3**–**5**, a linker of excessive length prevents the terminal ring from establishing stable polar interactions with the receptor. This is exemplified by compound **7**, whose oxothiazolidine group is positioned too externally relative to the receptor binding cavity. In contrast, a very short linker keeps the OTC group within the edges of the binding cavity, as detected for compound **6**. Docking results suggest that its oxothiazolidine ring replaces the amide function of **8** in making polar interaction with Ser67$^{2.65}$. The comparison of the docking-suggested interaction of compounds **6**–**8** with the hA_{2A} AR is reported as well in the Supplementary Data (Fig. S7).

The synthesized compounds present lower or null affinity at the

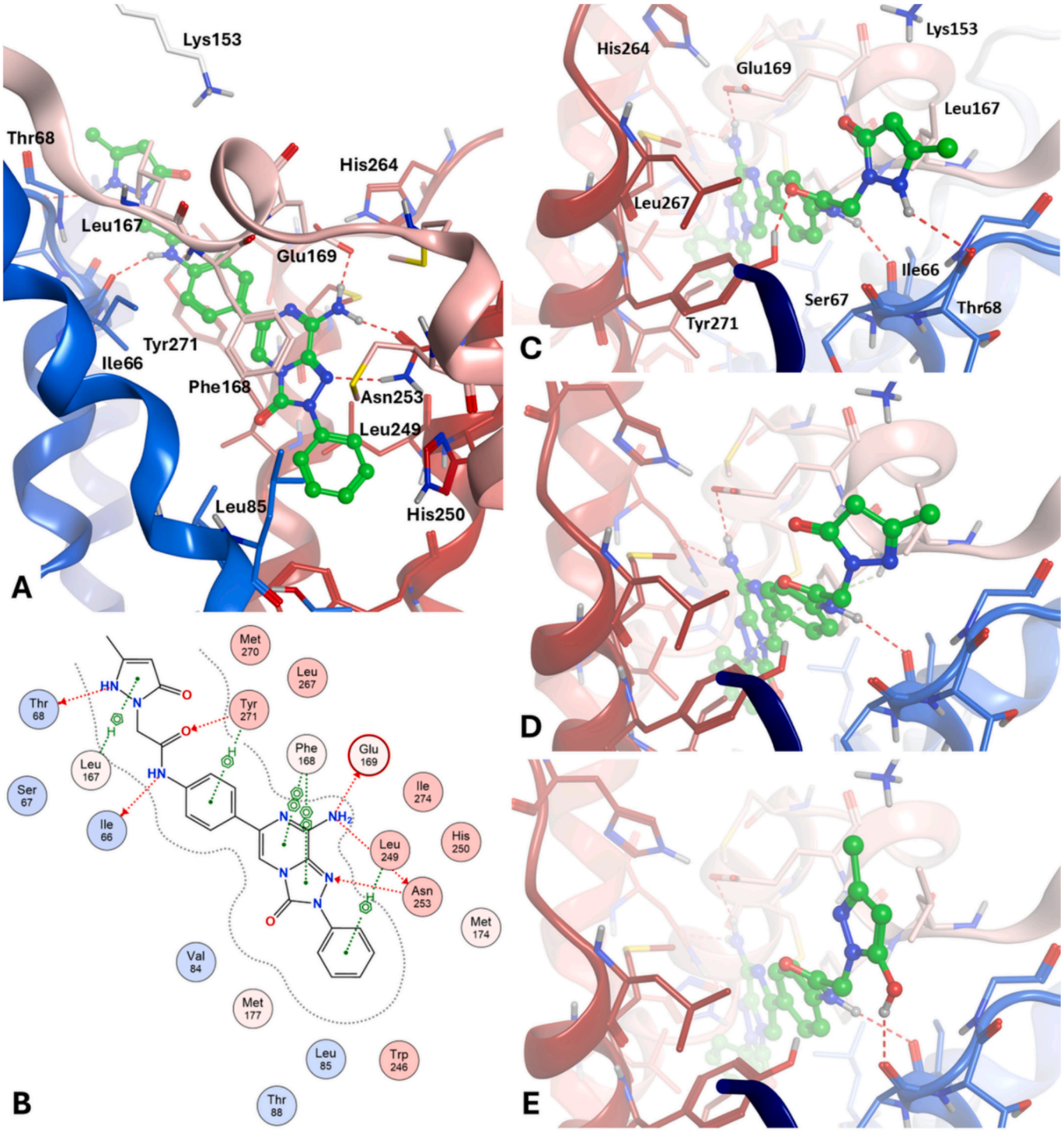

Fig. 5. Simulated conformations at the hA_{2A} AR. **A**: the binding mode of the EDA-containing compound **3** is shown (EL4 domain is hidden for clarity). **B**: schematic plot of ligand-target interaction. **C-E**: interaction of the 1H-pyrazol-3(2H)-one moiety (tautomer B, panel C) and its tautomers (tautomers A and C, respectively in panels D and E) with the receptor residues in their proximity.

other AR subtypes than hA_{2A} AR. We hence performed a docking analysis at hA_1 and hA_3 ARs binding sites to analyze the interaction between these receptors and the new derivatives. For this analysis, we employed a crystal structure of the hA_1 AR (pdb code: 5N2S; 3.3-Å resolution [41]) and a cryo-EM structure of the hA_3 AR (pdb code: 8X16; 3.3-Å resolution [42]), which were checked and if necessary restored in their wild type sequence and added of hydrogen atoms. As shown in Fig. 7, the potential interaction of the novel compounds with hA_1 and hA_3 ARs is analogous to that observed with the hA_{2A} AR, although some minor differences are present. The polar interactions with hA_1 AR Asn254$^{6.55}$ and Glu172 (EL2) mimic the ones with Asn253$^{6.55}$ and Glu169 (EL2) at the hA_{2A} AR, as well as the π-π stacking with Phe171 (EL2, hA_1 AR, corresponding to Phe168 in hA_{2A} AR). At the external region of the hA_1 AR, Glu170 (EL2) replaces the hA_{2A} AR Leu167 residue. This takes to a different interaction with the substituent in the 6-position. While at the hA_{2A} AR i.e. the pyrazolone ring could provide an H-bond donor function to give polar interaction with TM2 residues like Ser67$^{2.65}$ or Thr68$^{2.66}$ together with non-polar interaction with Leu167 (Fig. 5), at the hA_1 AR the presence of

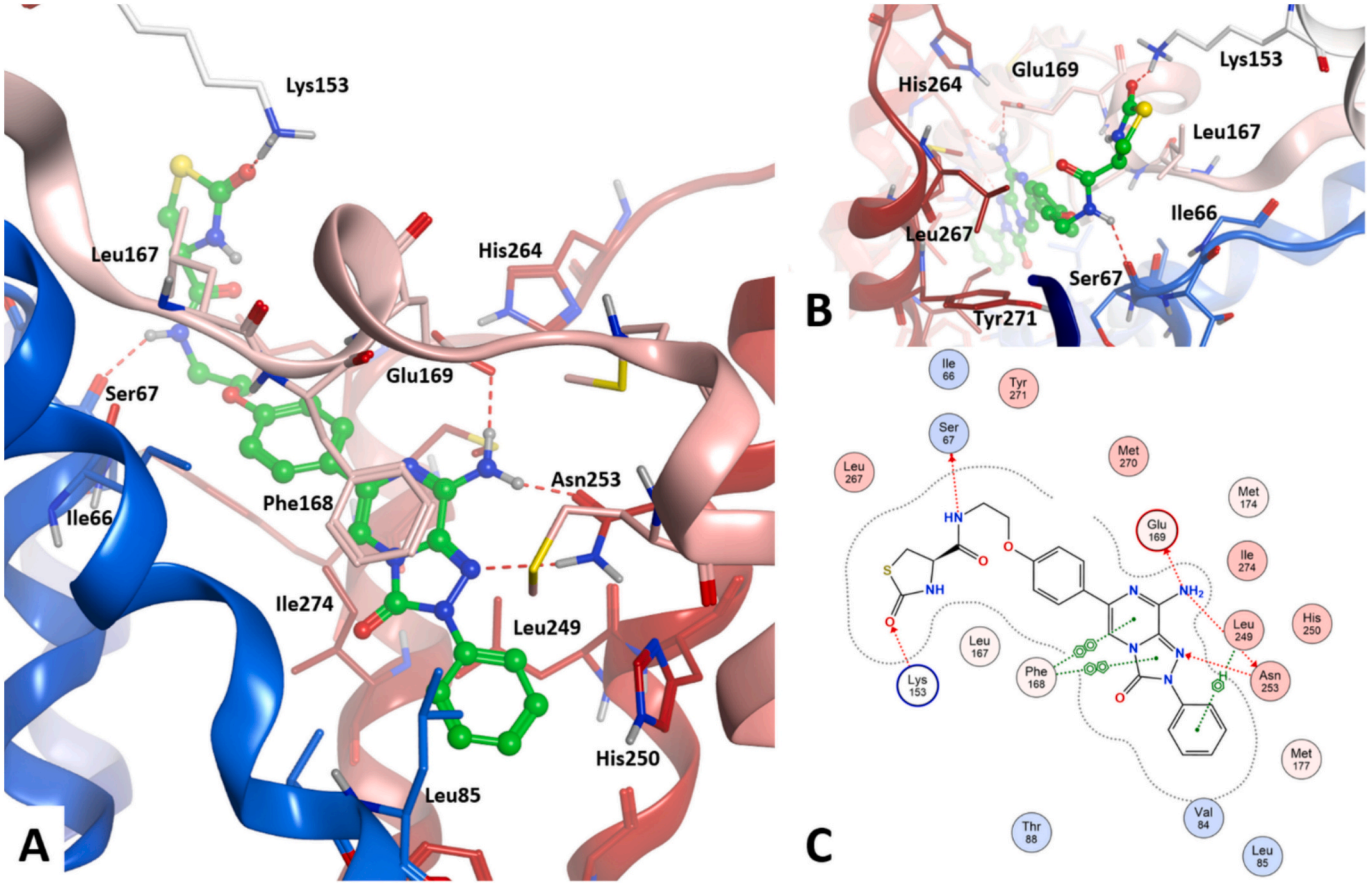

Fig. 6. Simulated conformations at hA_{2A} AR. Left: the binding mode of the OTC-containing compound **8** is shown (EL4 domain is hidden for clarity). Top and bottom right: top view and schematic plot of ligand-target interaction.

Glu170 in the EL2 domain makes the pyrazolone ring able to give such polar interaction just with this residue or with polar residues in the TM2 domain (Fig. 7).

On the other hand, the non-polar interaction previously seen at hA_{2A} AR is lacking at the hA_1 AR. This could help explain, at least in part, the generally lower affinity of the EDA-containing compounds for the latter receptor. Furthermore, as observed at the hA_{2A} AR, the length of the linker appears also critical for the affinity at hA_1 AR, with compound **4** being the only one showing hA_1 AR affinity among the EDA-containing molecules. Docking results suggest that in the presence of a shorter linker (derivative **3**) the molecule is forced to move externally from the general position in the binding site (i.e. the one adopted by compound **4**) to restore polar interaction with TM2 residues like $Asn70^{2.65}$, but this takes to a partial loss of polar interaction with $Asn254^{6.55}$. This could explain the drop of affinity at this receptor for compound **3**. Same suggestions are given for compound **5**, whose linker has analogue length compared to compound **3**. The comparison of docking conformations of compounds **3**–**5** at the hA_1 AR is reported in the Supplementary Data (Fig. S8). Some hA_1 AR affinity is restored for the OTC-containing compounds, in which the H-bond donor and acceptor groups of the oxothiazolidine make this group being oriented toward the above-cited EL2 residue Glu170 as well as the EL2 residue Lys173 (see docking conformation of compound **8** at the hA_1 AR, Fig. 7, and Fig. S9 in Supplementary Data). Even in this case, the length of the linker appears critical, as a shorter linker (i.e. compound **6**) makes the compound unable to give this double polar interaction with EL2 residues but able to give at least a polar contact with TM2 residues ($Asn70^{2.65}$). On the other hand, a longer linker (i.e. compound **7**) restores the polar interaction with Glu170 (EL2), but through the more external amide group instead of the oxothiazolidine ring.

At the hA_3 AR, the non-polar interaction with Phe168 (EL2) and the H-bond with $Asn250^{6.55}$ correspond to the analogue ones with Phe168 and $Asn253^{6.55}$ in hA_{2A} AR. In contrast, the additional polar interaction with Glu169 (EL2) observed at the hA_{2A} AR is not possible at the hA_3 AR, since this residue is replaced in the latter receptor by a valine (Val169), which cannot give polar interaction with the amine group of the novel compounds. This is a main point related to the lower affinity at this receptor (Fig. 7). Though, in the position corresponding to Glu170 of hA_1 AR and Leu167 of hA_{2A} AR, it is present the residue Gln167, whose amide group in the side chain contains both H-bond donor and acceptor functions. As a consequence, the pyrazolone ring of compounds **3**–**5** can interact as an H-bond donor with TM2 residues and as an H-bond acceptor with Gln167 (Fig. S10 in Supplementary Data). The H-bond acceptor group of the oxothiazolidine ring in OTC-containing compounds can interact analogously with the same EL2 residue (i.e. compound **8,** Fig. S11 in Supplementary Data). However, the docking at the hA_3 AR do not provide a clear rationale for interpreting the biological data of the new compounds at this receptor.

2.6. Pharmacological studies

Some triazolopyrazine derivatives were selected to be evaluated in two different in vitro models of cerebral ischemia to determine their ability in reducing neuronal damage induced by oxygen and glucose deprivation (OGD). Acute hippocampal slices represent an in vitro model used to study electrophysiological events during global ischemia, where glutamate release triggers anoxic depolarization (AD) appearance and neuronal cell death. Whereas organotypic slice cultures were used as a complementary in vitro model of ischemia, in which the tissue structure and synaptic organization were preserved [43].

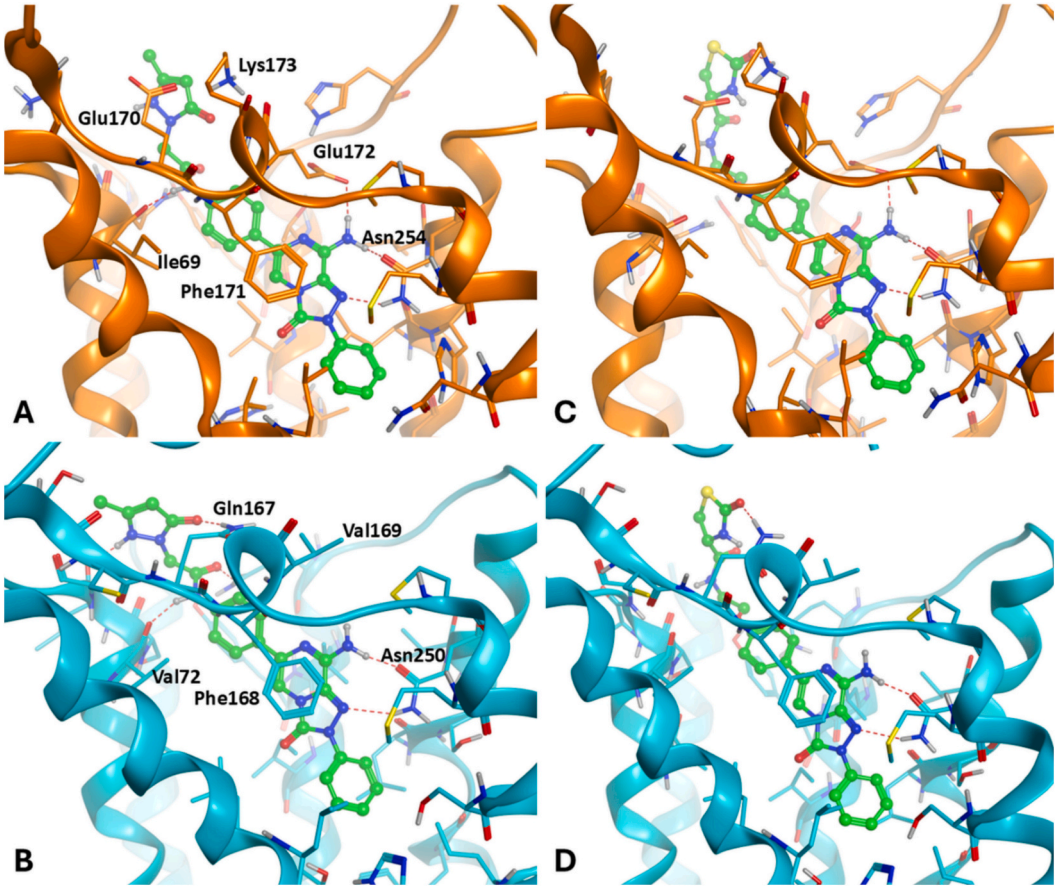

Fig. 7. Simulated conformations at hA_1 (orange) and hA_3 (blue) ARs. The binding modes of compound **3** (**A-B**) and compound **8** (**C—D**) are shown (EL4 domain is hidden for clarity). (For interpretation of the references to colour in this figure legend, the reader is referred to the web version of this article.)

*2.6.1. Antioxidant-hybridized A_{2A} AR antagonists **3, 4, 6** and **8** delay AD appearance in OGD-exposed acute hippocampal slices*

Derivatives **3**, **4** and **6**, **8**, respectively EDA- and OTC-hybridized, were evaluated for their effect on CA1 synaptic transmission during the application of a prolonged and severe OGD episode in acutely isolated hippocampal slices. Moreover, OTC, EDA, and compound **24**, a potent and selective A_{2A} AR antagonist from the triazolopyrazine series lacking the antioxidant moiety [17] (Table 1), were tested as reference compounds. Synaptic transmission was measured by the extracellular recording of the field excitatory postsynaptic potential (fEPSP). An episode of 30 min OGD is always able to induce AD onset, which is a clear indication of tissue damage that consistently appears, along with the permanent loss of neurotransmission [44]. As reported in Table 4, no effects on fEPSP amplitude (mV) were observed in the presence of each compound investigated, under normoxic conditions at the end of 15 min application.

Table 4
Effect of the antioxidant-hybridized hA_{2A} AR antagonists **3**, **4**, **6, 8** and the reference compounds **24**, EDA, and OTC on basal synaptic transmission in the CA1 region of acutely isolated hippocampal slices.

		fEPSP amplitude	
Compd (conc)	n	Before (ctrl) (mV)[a]	After drugs (mV)[a]
3 (200 nM)	8	1.08 ± 0.20	1.07 ± 0.20
4 (200 nM)	8	0.90 ± 0.21	0.91 ± 0.25
24 (100 nM)	8	0.94 ± 0.11	0.95 ± 0.11
EDA (200 nM)	6	1.02 ± 0.24	1.05 ± 0.25
6 (50 nM)	9	1.03 ± 0.19	1.08 ± 0.17
8 (200 nM)	5	1.05 ± 0.15	1.07 ± 0.17
OTC (50 nM)	5	1.38 ± 0.06	1.38 ± 0.07

[a] Each value represents the mean ± SD of fEPSP amplitude (expressed in mV) recorded immediately before (ctrl) or after 15 min drug application (drugs).

As shown in Fig. 8b, in this experimental series, 30 min OGD evoked appearance of AD, recorded as a negative extracellular direct current (d.c.) shift, with a mean latency of 6.31 ± 1.07 min and a mean peak amplitude of 7.61 ± 1.06 mV ($n = 18$) in untreated slices. In the presence of the EDA-hybridized compound **3** or **4**, both at the concentration of 200 nM, AD appearance was significantly delayed to 8.36 ± 1.54 min (Fig. 8c, g; $n = 8$) and to 8.10 ± 1.06 min (Fig. 8d, g; $n = 8$), respectively. The reference triazolopyrazine **24** (100 nM) also significantly postponed AD onset to 8.43 ± 1.67 min (Fig. 8e, g; $n = 8$), similarly to the effect observed in the presence of the canonical A_{2A} AR antagonist, ZM241385 [35]. Finally, EDA applied alone at a concentration of 200 nM delayed AD appearance with a mean latency of 8.0 ± 0.63 min (Fig. 8f, g; $n = 6$). No significant differences in AD amplitude were observed across the experimental groups (Fig. 8h). Overall, compounds that delay the occurrence and propagation of AD, such as **3** and **4**, can be considered neuroprotective being able to protect brain tissue after ischemia [45]. It has to be pointed out that compounds **3** and **4**, even though equiactive to **24** in delaying the occurrence of AD, were significantly less potent than **24** as hA_{2A} AR antagonists in the functional cAMP assays (Table 2). These findings suggest that the effect of **3** and **4** on AD could be due not only to the A_{2A} AR antagonistic property but also to the antioxidant one. To confirm this hypothesis, we tested **3** and **4** in a complementary in vitro model of cerebral ischemia (see paragraph 2.6.2).

In another experimental set, we assessed the effects of the OTC-hybridized antagonists **6** and **8** on AD development, and compared them to the effects observed with OTC alone. Compounds **6** and **8** did not modify basal CA1 synaptic transmission, as reported in Table 4. However, when tested during a severe OGD insult, the OTC-hybridized

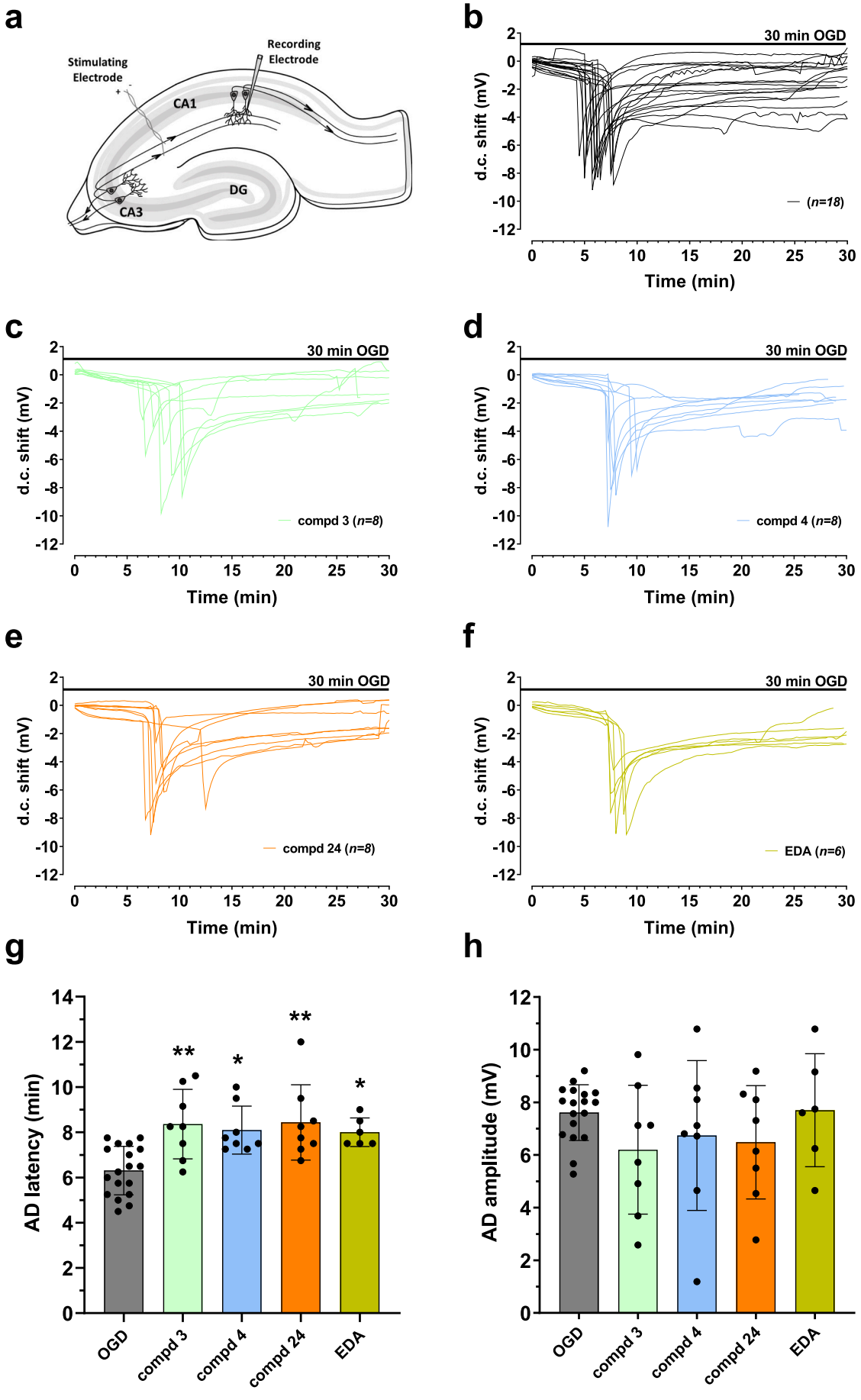

(caption on next page)

Fig. 8. Effects of derivatives compounds **3**, **4**, **24**, and EDA in acute rat CA1 hippocampal slices subjected to 30 min OGD. (a) Hippocampal slice diagram indicating the localization of the stimulating and recording electrodes. (b-f) Each graph shows voltage traces of direct current (d.c) shifts recorded during 30 min OGD in untreated OGD slices (b) or in the presence of different compounds: 200 nM compd **3**, 200 nM compd **4**, 100 nM compd **24** and 200 nM EDA (c-f). (g) Each column represents the mean ± SD of AD latency during 30 min OGD in different experimental groups. AD was measured from the beginning of the OGD insult. * $p < 0.05$, ** $p < 0.01$ vs. OGD, (ANOVA + Tukey's w-test). (h) Each column represents the mean ± SD of AD amplitude. The number (n) of slices tested is indicated inside the columns.

antagonists effectively delayed the onset of AD. As shown in Fig. 9a, e (*n = 11*), 30 min OGD elicited AD appearance with a mean latency of 6.31 ± 0.77 min and a mean peak amplitude of 6.22 ± 2.23 mV.

The application of the OTC-hybridized A_{2A} AR antagonists **6** (50 nM) or **8** (200 nM) significantly delayed the d.c. shift to 8.39 ± 1.86 min (Fig. 9b,e; $n = 9$) or to 8.70 ± 1.8 min, respectively (Fig. 9c, e; $n = 5$). In contrast, the application of OTC alone did not modify AD appearance (7.45 ± 0.54 min, Fig. 9d,e; $n = 5$). Additionally, no significant differences in AD amplitude were observed among the experimental groups (Fig. 9f). On this basis, for derivatives **6** and **8**, we may hypothesize that the major role in AD onset is played by the A_{2A} AR antagonist component, rather than the OTC portion.

The efficacy of the triazolopyrazines **3, 4, 6, 8** in this hippocampal model suggests that these compounds have physicochemical properties that enable effective tissue penetration, making them good candidates for in vivo studies in animal models of cerebral ischemia.

*2.6.2. EDA-hybridized A_{2A} AR antagonists **3** and **4** reduces CA1 injury in organotypic hippocampal slices exposed to OGD*

The effects of EDA-hybridized triazolopyrazines **3** and **4** on CA1 toxicity induced by 30 min OGD in rat organotypic hippocampal slices were investigated. Moreover, we tested the effects of EDA and the triazolopyrazine **24** [17] as reference compounds. Neuronal cell injury was assessed by measuring the intensity of propidium iodide (PI)

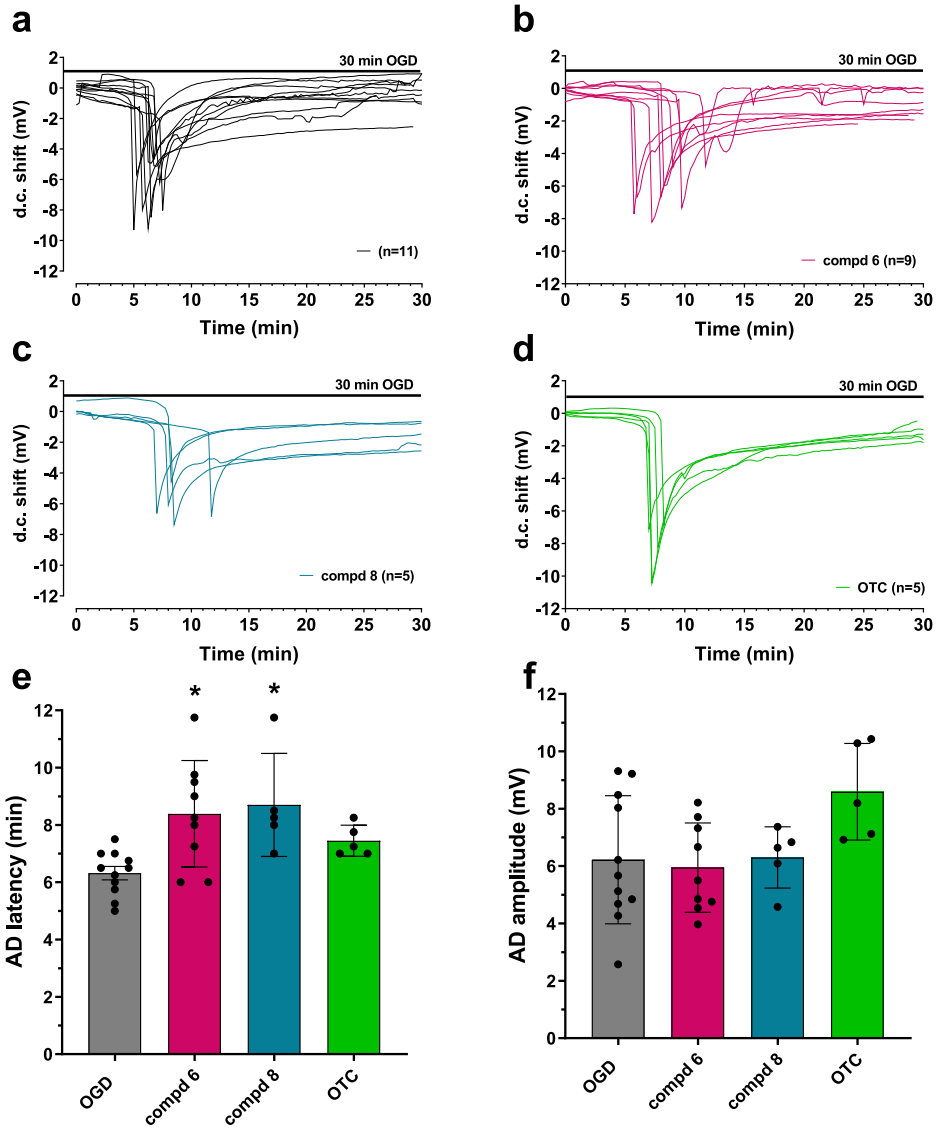

Fig. 9. Effects of derivatives **6**, **8,** and (*R*)-2-oxothiazolidine-4-carboxylic acid (OTC) in acute rat CA1 hippocampal slices exposed to 30 min OGD. (a-d) Each graph shows voltage traces of direct current (d.c) shifts recorded during 30 min OGD in untreated OGD slices (a) or in the presence of different compounds: 50 nM compd **6**, 200 nM compd **8**, 50 nM OTC (b-d). (e) Each column represents the mean ± SD of AD latency during 30 min OGD in different experimental conditions. AD was measured from the beginning of the OGD insult. *$p < 0.05$ vs. OGD, (ANOVA + Tukey's w-test) (f) Each column represents the mean ± SD of AD amplitude. The number (n) of slices tested is indicated inside the columns.

fluorescence. In basal conditions, rat organotypic hippocampal slices exposed to **3** and **4**, EDA and compound **24**, at the concentrations of 0.1–10 μM for 24 h displayed no apparent signs of injury (data not shown). When EDA-hybridized compounds **3** and **4** were incubated during OGD and the subsequent 24 h, they significantly reduced neuronal damage at concentrations of 1 and 10 μM (Fig. 10).

The reference compound EDA and derivative **24** reduced the CA1 injury, significantly only at 10 μM (Fig. 10). In contrast, compounds **3** and **4** showed more pronounced neuroprotective effects, compared to EDA and **24**, which could be attributed to the additive effects of their antioxidant properties and A_{2A} AR antagonistic activity.

3. Conclusion

A set of triazolopyrazine derivatives hybridized with the antioxidant EDA (compounds **1–5**) and the cysteine precursor OTC (compounds **6–8**) was designed to obtain A_{2A} AR antagonists endowed with antioxidant properties, as potential neuroprotective agents for the treatment of cerebral ischemia. On the whole, the new derivatives showed nanomolar hA_{2A} AR affinity ($K_i = 1.7–117$ nM) and good selectivity versus the other AR subtypes. Molecular docking studies revealed the best binding mode of the new compounds at the hA_{2A} AR crystal structure, with the 2-phenyl ring positioned in the depth of the receptor cavity, and the 6-substituent located at the entrance and oriented toward the extracellular environment. Molecular docking studies performed at the hA_1 AR and hA_3 AR provided some explanations for the general low affinity of the compounds at these AR subtypes.

Selected EDA-hybridized and OTC-conjugated derivatives, tested in in vitro hippocampus models of cerebral ischemia, resulted in potential neuroprotective agents. In particular, EDA-based derivatives **3** and **4**, effective as free-radical scavengers in the DPPH assay, proved to be protective on acutely isolated rat hippocampal slices under a severe ODG insult (30 min duration), since they postponed the onset of AD, indicating a delay in the progression of neuronal damage. Compounds **3** and **4** were evaluated in parallel experiments on rat organotypic hippocampal slices exposed to 30 min of OGD and followed by a 24-h recovery period. In this model, they showed a greater neuroprotective effect, compared to the reference EDA and the A_{2A} AR antagonist **24**. These findings suggested that the potentiated effect of **3** and **4** might be due to both their antioxidant and A_{2A} AR antagonist components. Future studies will aim to complement these data with cell-based assays to evaluate the antioxidant efficacy of the compounds in a translationally relevant context. The observed efficacy of the triazolopyrazines in in vitro hippocampal models suggests that these compounds possess favorable physicochemical properties that support effective tissue penetration and potential in vivo activity, particularly under ischemic conditions, where the blood–brain barrier (BBB) is compromised and allows increased permeability into brain tissue. These considerations make these compounds promising candidates for in vivo studies aimed at further validating the hypothesis that dual-acting antioxidant-A_{2A} AR antagonists may offer enhanced therapeutic potential as neuroprotective agents in cerebral ischemia and other oxidative stress-related disorders.

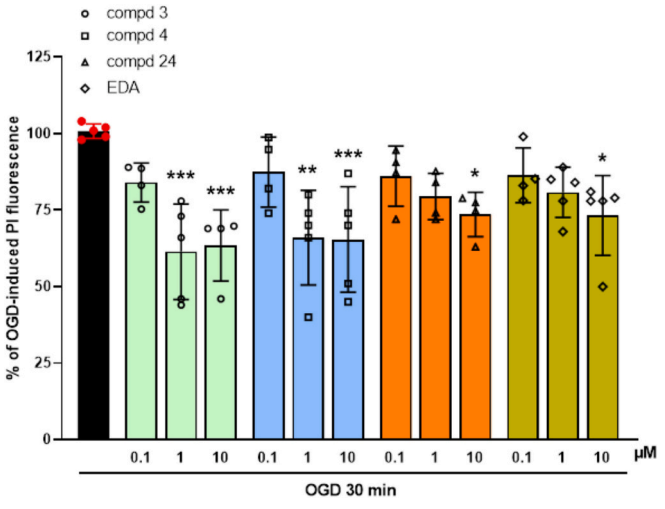

Fig. 10. Effects of compounds **3**, **4**, **24,** and EDA in organotypic slice cultures exposed to 30 min OGD. Quantitative analysis of the effects of **3**, **4**, **24,** and **EDA** during 30 min of OGD and in the subsequent 24 h of recovery. Bars represent the mean ± SD of at least four experiments run in quadruplicate. (* $p < 0.05$, ** $p < 0.01$ and *** $p < 0.001$ vs. OGD) (ANOVA + Tukey's w-test).

4. Experimental section

4.1. Chemistry

The microwave-assisted syntheses were performed using an Initiator EXP Microwave Biotage instrument (frequency of irradiation: 2.45 GHz). Analytical silica gel plates (0.20 mm, F254, Merck, Germany) and silica gel 60 (Merck, 70–230 mesh) were used for analytical and column chromatography, respectively. All melting points were determined on a Gallenkamp melting point apparatus and were uncorrected. The high-resolution mass spectrometry (HRMS) analysis was performed with a Thermo Finnigan LTQ Orbitrap mass spectrometer coupled with an electrospray ionization source (ESI). Analysis was carried out in positive ion mode $[M + H]^+$, and it was used a proper dwell time acquisition to achieve 60,000 units of resolution at full width at half maximum (FWHM). Elemental composition of compounds was calculated based on their measured accurate masses, accepting only results with an attribution error of less than 2 ppm and a not integer RDB (double bond/ring equivalents) value. The solvents used in MS measures were acetone, acetonitrile (Chromasolv grade), and mQ water 18 MΩ cm. Stock solutions of analytes were prepared using acetone (1.0 mg/mL) and stored at 4 °C. Then working solutions of each analyte were prepared by dilution of the stock solutions using mQ water/acetonitrile 1/1 (*v*/v) up to a concentration of 1.0 μg/mL The HRMS analysis was performed by introducing the analyte working solution via syringe pump at 10 μL min^{-1}. Elemental analyses were performed with a Flash E1112 Thermofinnigan elemental analyzer for C, H, N and the results were within 0.4 % of the theoretical values (Table S4). All final compounds revealed purity not less than 95 %. NMR spectra were recorded on a Bruker Avance 400 spectrometer (400 MHz for ^{1}H- and 100 Mz for ^{13}C NMR). The chemical shifts are reported in δ (ppm) and are relative to the central peak of the solvent which was $CDCl_3$ or $DMSOd_6$. The following abbreviations are used: s = singlet, d = doublet, t = triplet, q = quartet, m = multiplet, br = broad, and ar = aromatic protons. Scanned ^{1}H- and ^{13}C-NMR spectra of selected derivatives are reported in Supplementary Data.

4.1.1. *N-(4-(8-amino-3-oxo-2-phenyl-2,3-dihydro-[1,2,4]triazolo[4,3-a]pyrazin-6-yl)phenyl)-4-(3-methyl-5-oxo-4,5-dihydro-1H-pyrazol-1-yl) benzamide (1)*

Ethyl acetoacetate (1.65 mmol) was added to a solution of the hydrazine derivative **13** (1.65 mmol) in DCM (10 mL) and the mixture was heated at 60 °C for 2 h. The solvent was removed under reduced pressure and the crude product was treated with water (20 mL). The obtained solid was collected by filtration and purified by recrystallization from MeOH. Yield 58 %; mp 229–230 °C. ^{1}H NMR (DMSO-d_6) (tautomer B/tautomer A ratio about 7:1) 10.32 (br s, 1H, NH), 8.10–8.07 (m, 4H, ar), 7.98 (d, 2H, ar, $J = 7.7$ Hz), 7.91 (d, 2H, ar, $J = 8.8$ Hz), 7.86 (d, 2H, ar, $J = 8.8$ Hz), 7.76 (s, 1H, H_5), 7.59–7.57 (m, 4H, 2ar + NH_2), 5.41 (s, 1H, H_4 pyrazole tautomer B), 3.71 (s, 2H, CH_2 pyrazole tautomer A), 2.16 (s, 3H, CH_3). ^{13}C NMR 165.29, 149.93, 147.85, 147.61, 141.69, 139.68, 137.94, 135.27, 131.66, 131.59, 131.05, 130.59, 129.68, 129.23, 129.13, 126.81, 126.29, 120.60, 119.88, 119.39, 117.34, 101.37, 43.63, 17.19, 14.46. ESI-HRMS on $[C_{28}H_{23}N_8O_3]^+$ species found *m/z*

519.1894. Anal. Calc. for $C_{28}H_{22}N_8O_3$.

4.1.2. N-(2-(4-(8-amino-3-oxo-2-phenyl-2,3-dihydro-[1,2,4]triazolo[4,3-a]pyrazin-6-yl)phenoxy)ethyl)-4-(3-methyl-5-oxo-4,5-dihydro-1H-pyrazol-1-yl)benzamide (2)

Trifluoroacetic acid (4.30 mmol) was added to a suspension of the *N*-Boc-hydrazine derivative **12** (1.81 mmol) in anhydrous DCM (5 mL). The resultant red solution was stirred at rt. for about 1 h, until the disappearance of the starting material (TLC monitoring). The intermediate hydrazine derivative was not isolated but was promptly reacted with ethyl acetoacetate (1.65 mmol) added to the mixture. After heating at 60 °C for 2 h, the solvent was removed under reduced pressure and the crude product was treated with water (20 mL). The obtained solid was collected by filtration and purified by silica gel column chromatography (eluent EtOAc 4/cyclohexane 6/MeOH 1). Yield 32 %; mp > 300 °C. ^{1}H NMR (DMSO-d_6) (tautomer B) 8.71 (t, 1H, NH), 8.08 (d, 2H, ar, J = 8.0 Hz), 7.93–7.88 (m, 6H, ar), 7.67 (s, 1H, H_5), 7.56 (m, 4H, 2 ar + NH_2), 7.36 (t, 1H, ar, J = 7.3 Hz,), 7.03 (d, 2H, ar, J = 8.7 Hz), 5.34 (br s, 1H, H_4 pyrazole), 4.18 (t, 2H, CH_2, J = 6.2 Hz), 3.67 (q, 2H, CH_2, J = 5.4 Hz), 2.12 (s, 3H, CH_3). ESI-HRMS on $[C_{30}H_{27}N_8O_4]^+$ species found *m/z* 563.2139. Anal. Calcd. for $C_{30}H_{26}N_8O_4$.

4.1.3. N-(4-(8-amino-3-oxo-2-phenyl-2,3-dihydro-[1,2,4]triazolo[4,3-a]pyrazin-6-yl)phenyl)-2-(3-methyl-5-oxo-4,5-dihydro-1H-pyrazol-1-yl)acetamide (3)

Ethyl acetoacetate (0.21 mmol) was added to a suspension of the hydrazine derivative **17** (0.21 mmol) in absolute EtOH (4 mL) and catalytic AcOH (3 drops). The mixture was refluxed for 2 h, then cooled at rt. and the precipitate was collected by filtration, rinsed with EtOH (5 mL), and collected by filtration and recrystallized. Yield 40 %; mp 289–290 °C (EtOH). ^{1}H NMR (DMSO-d_6) (tautomer B/tautomer A ratio about 4:1) 10.84 (br s, 1H, NH pyrazole tautomer B), 10.26 (br s, 1H, NH), 8.08 (d, 2H, ar, J = 7.9 Hz,), 7.94 (d, J = 8.3 Hz, 2H, ar), 7.73 (s, 1H, H_5), 7.64 (d, 2H, ar, J = 8.3 Hz,), 7.59–7.55 (m, 4H, 2 ar + NH_2), 7.36 (t, 1H, ar, J = 7.6 Hz), 5.19 (s, 1H, H_4 pyrazole tautomer B), 4.61 (s, 2H, CH_2 tautomer B), 4.40 (s, 2H, CH_2 tautomer A), 3.46 (s, 2H, CH_2 pyrazole tautomer A), 2.02 (s, 3H, CH_3). ^{13}C NMR 173.53, 166.30, 156.94, 147.81, 147.62, 139, 06, 137.97, 135.66, 131.56, 129.64, 129.21, 126.74, 126.45, 119.86, 119.42, 118.72, 101.16, 47.44, 41.32, 16.98. ESI-HRMS on $[C_{23}H_{21}N_8O_3]^+$ species found *m/z* 457.1738. Anal. Calc. for $C_{23}H_{20}N_8O_3$.

4.1.4. N-(4-(8-amino-3-oxo-2-phenyl-2,3-dihydro-1,2,4-triazolo[4,3-a]pyrazin-6-yl)phenyl)-3-(3-methyl-5-oxo-4,5-dihydro-1H-pyrazol-1-yl)propenamide (4)

Ethyl acetoacetate (0.42 mmol) was added to a suspension of the hydrazine derivative **18** (0.42 mmol) in EtOH (20 mL) and the mixture was heated at 60 °C for 2 h. After cooling at room temperature, the solid was filtered off and the ethanolic solution was evaporated under reduced pressure. The obtained residue was taken up with Et_2O (20 mL) and the solid was collected by filtration. The crude product was purified by silica gel column chromatography (eluent $CHCl_3$ 9/MeOH 1). Yield 56 %; m.p. 250–254 dec °C. ^{1}H NMR (DMSO-d_6) (tautomer B) 10.74 (br s, 1H, NH pyrazole), 10.10 (s, 1H, NH), 8.06 (d, 2H, ar, J = 7.6 Hz), 7.90 (d, 2H, ar, J = 8.7 Hz), 7.70 (s, 1H, H-5), 7.63 (d, 2H, ar, J = 8.7 Hz), 7.54–7.59 (m, 4H, ar + NH_2), 7.35 (t, 1H, ar, J = 7.4 Hz), 5.14 (s, 1H, H4 pyrazole), 4.05 (m, 2H, CH_2), 2.77 (m, 2H, CH_2), 2.01 (s, 3H, CH_3). ESI-HRMS on $[C_{24}H_{23}N_8O_3]^+$ species found *m/z* 471.1897. Anal. Calc. for $C_{24}H_{22}N_8O_3$.

4.1.5. 8-Amino-6-(4-(2-(3-methyl-5-oxo-4,5-dihydro-1H-pyrazol-1-yl)ethoxy)phenyl)-2-phenyl-1,2,4-triazolo[4,3-a]pyrazin-3(2H)-one (5)

It was prepared from **21** (0.26 mmol) in the same experimental conditions described above to prepare derivative **3**. The crude product was purified by column chromatography (eluent CH_2Cl_2 10/MeOH 0.5). Yield 32 %; mp 215–217 °C. ^{1}H NMR (DMSO-d_6) (tautomer B) 10.75 (br s, 1H, NH pyrazole), 8.08 (d, 2H, ar, J = 7.7 Hz,), 7.90 (d, 2H, ar, J = 8.6 Hz), 7.66 (s, 1H, H_5), 7.58–7.54 (m, 4H, 2 ar + NH_2), 7.36 (t, 1H, ar, J = 7.2 Hz,), 6.96 (d, 2H, ar, J = 8.5 Hz), 5.16 (s, 1H, H_4 pyrazole), 4.29 (t, 2H, CH_2, J = 4.9 Hz,), 4.13 (t, 2H, CH_2, J = 4.9 Hz,), 2.02 (s, 3H, CH_3). ESI-HRMS on $[C_{23}H_{22}N_7O_3]^+$ species found *m/z* 444.1771. Anal. Calcd. for $C_{23}H_{21}N_7O_3$.

4.1.6. General procedure for the synthesis of the OTC-conjugated 8-amino-3-oxo-2-phenyl-2,3-dihydro-1,2,4-triazolo[4,3-a]pyrazine derivatives 6–8

A mixture of the suitable amino derivatives **9** [29], **21** [17] or **10** [29] (1 mmol), (*R*)-2-oxothiazolidine-4-carboxylic acid [35] (2 mmol), EDCI hydrochloride (2 mmol), HOBt (2 mmol), DIPEA (2 mmol) in anhydrous DMF (3 mL) was reacted, under nitrogen atmosphere, at 60 °C per 18 h, to obtain **6** and **8**, and at room temperature for 48 h, to prepare **7**. The mixture was diluted with water (20 mL) and the obtained solid was collected by filtration and purified as indicated below.

4.1.6.1. (R)-N-(4-(8-Amino-3-oxo-2-phenyl-2,3-dihydro-1,2,4-triazolo[4,3-a]pyrazin-6-yl)phenyl)-2-oxothiazolidine-4-carboxamide (6).

Purified by silica gel column chromatography (eluent $CHCl_3$ 9.4/ MeOH 0.6). Yield 75 %; mp > 300 °C. ^{1}H NMR (DMSO-d_6) 10.26 (s, 1H, NH), 8.37 (s, 1H, NH), 8.08 (d, 2H, ar, J = 8.0 Hz), 7.96 (d, 2H, ar, J = 8.6 Hz), 7.73 (s, 1H, ar), 7.68 (d, 2H, ar, J = 8.6 Hz), 7.56 (br. s, 2H, NH_2), 7.56 (t, 2H, ar, J = 8.0 Hz), 7.35 (t, 1H, ar, J = 7.3 Hz), 4.51–4.48 (m, 1H, CH), 3.80–3.75 (m, 1H, CH), 3.49–3.53 (m, 1H, CH). ^{13}C NMR (DMSO-d_6) 174.06; 169.11; 147.83; 147.62; 138.90; 137.96; 135.56; 132.18; 131.56; 129.66; 126.76; 126.44; 119.84; 119.71; 101.26; 57.49; 32.79. ESI-HRMS on $[C_{21}H_{18}N_7O_3S]^+$ species found *m/z* 448.1189. Anal. Calcd for $C_{21}H_{17}N_7O_3S$.

4.1.6.2. (R)-N-(3-((4-(8-amino-3-oxo-2-phenyl-2,3-dihydro-1,2,4-triazolo[4,3-a]pyrazin-6-yl)phenyl)amino)-3-oxopropyl)-2-oxothiazolidine-4-carboxamide (7).

Purified by silica gel column chromatography (CH_2Cl_2 9/MeOH 0.6). Yield 25 %; mp 167–169 °C (EtOH/2-Methoxyethanol). ^{1}H NMR (DMSO-d_6) δ 10.07 (s, 1H, NH), 8.29 (s, 1H, NH), 8.20–8.21 (m, 1H, NH), 8.29 (d, 2H, ar, J = 8.01 Hz), 7.96 (d, 2H, ar, J = 8.6 Hz), 7.70 (s, 1H, H-5), 7.66 (d, 2H, ar, J = 8.6 Hz), 7.59–7.56 (m, 4H, ar + NH_2), 7.36 (t, 1H, ar, J = 7.3 Hz), 4.29–4.26 (m, 1H, CH), 3.69–3.62 (m, 1H, CH), 3.44–3.40 (m, 3H, CH + CH_2), 2.55–2.50 (m, 2H, CH_2). ^{13}C NMR (DMSO-d_6) 173.80, 170.50, 169.83, 147.79, 147.62, 139.50, 137.97, 135.72, 131.56, 129.66, 126.32, 119.86, 119.41, 104.04, 56.74, 36.55, 35.78, 32.81. ESI-HRMS on $[C_{24}H_{23}N_8O_4S]^+$ species found m/z 519.1558.Anal. Calcd for $C_{24}H_{22}N_8O_4S$.

4.1.6.3. (R)-N-(2-(4-(8-amino-3-oxo-2-phenyl-2,3-dihydro-1,2,4-triazolo[4,3-a]pyrazin-6-yl)phenoxy)ethyl)-2-oxothiazolidine-4-carboxamide (8)..

Purified by recrystallization. Yield 85 %; mp 256–257 dec °C (EtOH/2-Methoxyethanol). ^{1}H NMR (DMSO-d_6) 8.37 (t, 1H, NH, J = 5.4 Hz), 8.32 (br s, 1H, NH), 8.07 (d, 2H, ar, J = 7.8 Hz), 7.92 (d, 2H, ar, J = 8.8 Hz), 7.67 (s, 1H, H-5), 7.58–7.54 (m, 4H, 2ar + NH_2), 7.35 (t, 1H, ar, J = 7.4 Hz), 7.00 (d, 2H, ar, J = 8.9 Hz), 4.34–4.31 (m, 1H, CH), 4.07 (t, 2H, CH_2, J = 5.5 Hz), 3.70–3.65 (m, 1H, CH), 3.51 (q, 2H, CH_2, J = 5.5 Hz), 3.36–3.32 (m, 1H, CH). ESI-HRMS on $[C_{23}H_{22}N_7O_4S]^+$ species found m/z 492.1455. Anal. Calcd for $C_{23}H_{21}N_7O_4S$.

4.1.7. General procedure for the synthesis of the N-Boc hydrazino derivatives 11 and 12

A mixture of *N*-Boc-4-hydrazinobenzoic acid [30] (2.07 mmol) and Et_3N (2.07 mmol) in anhydrous DMF (2 mL) was stirred at r.t. for about 15 min. Then, EDC hydrochloride (2.07 mmol) and HOBt (2.07 mmol) were added and, after 10 min, the suitable amino derivative **9** and **10** (2.07 mmol) was added. The reaction was heated at 35 °C for 48 h and 24 h to give, respectively, **11** and **12**. After cooling at r.t., the mixture was diluted with water (20 mL) and the obtained solid was collected by filtration and used in the next step without further purification.

*4.1.7.1. Tert-butyl 2-(4-((4-(8-amino-3-oxo-2-phenyl-2,3-dihydro-1,2,4-triazolo[4,3-a]pyrazin-6-yl)phenyl)carbamoyl)phenyl)hydrazine-1-carboxylate **(11)**.* Yield 81 %. ^{1}H NMR (DMSO-d_6) 9.99 (s, 1H, NH), 8.93 (s, 1H, NH), 8.16 (s, 1H, NH), 8.08 (d, 2H, ar, J = 7.9 Hz,), 7.95 (d, 2H, ar, J = 8.7 Hz), 7.83 (d, 2H, ar, J = 8.7 Hz), 7.73 (s, 1H, H5), 7.57–7.55 (m, 4H, 2ar + NH_2), 7.36 (t, 1H, ar, J = 7.4 Hz,), 6.72 (d, 2H, ar, J = 8.6 Hz,), 1.44 (s, 9H, tert-butyl).

*4.1.7.2. Tert-butyl 2-(4-((2-(4-(8-amino-3-oxo-2-phenyl-2,3-dihydro-[1,2,4]triazolo[4,3-a]pyrain-6-yl)phenoxy)ethyl)carbamoyl)phenyl)hydrazine-1-carboxylate **(12)**.* Yield 75 %. ^{1}H NMR (DMSO-d_6) 8.88 (br s, 1H, NH), 8.36 (br s, 1H, NH), 8.09–8.04 (m, 2H, ar + NH), 7.91 (d, 2H, ar J = 8.7 Hz,), 7.71 (d, 2H, ar J = 8.3 Hz,), 7.66 (s, 1H, H_5), 7.58–7.55 (m, 4H, ar + NH_2), 7.37 (t, 1H, ar, J = 7.4 Hz,), 7.02 (d, 2H, ar, J = 8.9 Hz), 6.65 (d, 2H, ar, J = 8.7 Hz,), 4.14 (t, 2H, CH_2, J = 6.5 Hz), 3.60–3.63 (m, 2H, CH_2), 1.42 (s, 9H, tert-butyl).

*4.1.8. N-(4-(8-amino-3-oxo-2-phenyl-2,3-dihydro-1,2,4-triazolo[4,3-a]pyrazin-6-yl)phenyl)-4-hydrazinylbenzamide **(13)***

To a suspension of *N*-Boc-hydrazino derivatives **11** (6.87 mmol) in anhydrous DCM, TFA (8.25 mmol) was added. The resulting dark solution was stirred at r.t. for 22 h, then the solvent was evaporated under reduced pressure. The obtained residue was treated with H_2O (20 mL) and the pH was adjusted to 7 with a saturated solution of $NaHCO_3$. The resulting suspension was extracted with EtOAc (3 × 20 mL). The organic phase was anhydrified (Na_2SO_4) and the solvent was evaporated under reduced pressure to give a crude solid which was used in the next step without purification. Yield 51 %. ^{1}H NMR (DMSO-d_6) 9.89 (s, 1H, NHCO), 8.09 (d, 2H, ar, J = 7.9 Hz), 7.94 (d, 2H, ar, J = 8.7 Hz), 7.85–7.80 (m, 4H, ar), 7.73 (s, 1H, H_5), 7.59–7.55 (m, 4H, ar + NH_2), 7.40–7.36 (m, 2H, ar), 6.81 (d, 2H, ar, J = 8.6 Hz), 4.19 (br s, 2H, NH_2).

*4.1.9. N-(4-(8-amino-3-oxo-2-phenyl-2,3-dihydro-1,2,4-triazolo[4,3-a]pyrazin-6-yl)phenyl)-2-chloroacetamide **(14)***

A mixture of **9** (0.31 mmol), chloroacetic acid (0.28 mmol), EDCI hydrochloride (0.31 mmol) and HOBt (0.31 mmol) in anhydrous DMF (1 mL) was stirred overnight at rt. The mixture was diluted with water (20 mL) and the obtained solid was collected by filtration. The crude product was used without further purification. Yield 55 %. ^{1}H NMR (DMSO-d_6) 10.40 (s, 1H, NH), 8.08 (d, 2H, ar, J = 7.9 Hz), 7.96 (d, 2H, ar, J = 8.6 Hz), 7.73 (s, 1H, ar), 7.66 (d, 2H, ar, J = 8.6 Hz), 7.59–7.55 (m, 4H, ar + NH_2), 7.36 (t, 1H, J = 7.3 Hz), 4.28 (s, 2H, CH_2).

*4.1.10. N-(4-(8-amino-3-oxo-2-phenyl-2,3-dihydro-[1,2,4]triazolo[4,3-a]pyrazin-6-yl)phenyl)acrylamide **(15)***

The title compound **15** was synthesized as previously reported [17], i.e. by reacting the amino derivative **9** with 3-chloropropionic acid in the same experimental conditions reported above to prepare **14** from **9**.

*4.1.11. N-(4-(8-amino-3-oxo-2-phenyl-2,3-dihydro-1,2,4-triazolo[4,3-a]pyrazin-6-yl)phenyl)-2-hydrazinylacetamide **(16)***

Anhydrous hydrazine (58 mmol) was added to a suspension of the chloro derivative **14** (1.47 mmol) in absolute EtOH (10 mL) and the mixture was refluxed for 1 h. After cooling at r.t., the precipitate was collected by filtration and rinsed with EtOH (10 mL). The crude compound was pure enough to be used for the next step without further purification. Yield 68 %. ^{1}H NMR (DMSO-d_6) 9.89 (br s, 1H, NH), 8.08 (d, 2H, ar, J = 7.9 Hz), 7.93 (d, 2H, ar, J = 8.6 Hz), 7.72–7.70 (m, 3H, 2ar + H_5), 7.58–7.54 (m, 4H, 2ar + NH_2), 7.35 (t, 1H, ar J = 7.5 Hz), 3.88 (br, 3H, $NHNH_2$), 3.38 (s, 2H, CH_2).

*4.1.12. N-(4-(8-amino-3-oxo-2-phenyl-2,3-dihydro-1,2,4-triazolo[4,3-a]pyrazin-6-yl)phenyl)-3-hydrazinylpropanamide **(17)***

Hydrazine monohydrate (13.4 mmol) was added to a suspension of the acrylamide derivative **15** (0.54 mmol) in anhydrous THF (10 mL) and the resulting mixture was refluxed for 25 h. The solvent was eliminated under reduced pressure and the residue was treated with Et_2O (20 mL). The obtained solid was collected by filtration and recrystallized. Yield 78 % (nitromethane); mp 208–210 °C ^{1}H NMR (DMSO-d_6) 10.17 (s, 1H, NHCO), 8.93 (br s, 1H, NH), 8.08 (d, 2H, ar, J = 7.6 Hz), 7.91 (d, 2H, ar, J = 8.7 Hz), 7.63–7.69 (m, 3H, ar + H-5), 7.54–7.58 (m, 4H, 2ar + NH_2), 7.35 (t, 1H, ar, J = 7.4 Hz), 2.91 (t, 2H, CH_2, J = 6.7 Hz), 2.48 (t, 2H, CH_2, J = 6.7 Hz). ESI-HRMS on $[C_{20}H_{21}N_8O_2]^+$ species found *m/z* 405.1779. Anal. Calcd. for $C_{20}H_{20}N_8O_2$.

*4.1.13. 8-Amino-6-(4-(2-bromoethoxy)phenyl)-2-phenyl-[1,2,4]triazolo[4,3-a]pyrazin-3(2H)-one **(19)***

Triphenylphosphine (2.6 mmol) and *N*-bromosuccinimide (2.6 mmol) were added to a cold (T = 0 °C) suspension of the idrossi derivative **18** [31] (1.04 mmol) in anhydrous DCM (50 mL). The resulting mixture was heated at 60 °C for 24 h. After cooling at rt., the suspension was diluted with H_2O (20 mL) and extracted with DCM (30 mL × 3). The organic phase was washed with NaCl saturated solution of (50 mL × 3) and dried (Na_2SO_4). After elimination of the solvent under reduced pressure, a solid was obtained which was suspended in toluene (2 mL) to remove the excess of triphenylphosphine oxide. The solid residue was collected by filtration and used for the next step without further purification. Yield 50 %. ^{1}H NMR (DMSO-d_6) 8.07 (d, 2H, ar, J = 7.7 Hz), 7.92 (d, 2H, ar, J = 8.8 Hz), 7.68 (s, 1H, H_5), 7.55–7.57 (m, 4H, 2ar + NH_2), 7.35 (t, 1H, ar, J = 7.4 Hz), 7.02 (d, 2H, ar, J = 8.9 Hz), 4.37 (t, 2H, CH_2, J = 5.4 Hz), 3.83 (t, 2H, CH_2, J = 5.4 Hz).

*4.1.14. 8-Amino-6-(4-(2-hydrazineylethoxy)phenyl)-2-phenyl-1,2,4-triazolo[4,3-a]pyrazin-3(2H)-one **(20)***

Anhydrous hydrazine (58 mmol) was added to a mixture of **20** (1.47 mmol) in absolute EtOH (10 mL) and the obtained suspension was refluxed for 24 h. The insoluble was collected by filtration and rinsed with EtOH (10 mL) and used for the next step without further purification. Yield 40 %. ^{1}H NMR (DMSO-d_6) 8.08 (d, 2H, ar, J = 8.1 Hz), 7.90 (d, 2H, ar, J = 8.4 Hz), 7.66 (s, 1H, H_5), 7.58–7.54 (m, 4H, 2ar + NH_2), 7.36 (t, 1H, ar, J = 7.5 Hz), 6.99 (d, 2H, ar, J = 8.2 Hz), 4.09 (t, 2H, CH_2, J = 5.2 Hz), 3.83 (br, 3H, $NHNH_2$), 2.98 (t, 2H, CH_2, J = 5.1 Hz).

4.2. DPPH assay

4.2.1. DPPH free radical scavenging activity assay

The radical scavenging activity of the compounds was measured following a slightly modified previously reported procedure [36]. A fresh solution of $1\bullet10^{-4}$ M $DPPH^\bullet$ in methanol was prepared and kept in the dark at room temperature for 1 h. Ascorbic acid, EDA and the synthesized compounds were dissolved in DMSO for the preparation of stock solutions ($2\bullet10^{-4}$ M). The stock solutions were gradually diluted with MeOH to obtain an aliquot of 1000 μL of synthesized compounds solutions at different concentrations mixed with 1000 μL of DPPH solution in UV cuvettes (UV Transparent Disponsable Cuvettes (for use form 200 nm)-Sarsted). The mixtures were incubated for 30 min in the dark at room temperature. After this time, the absorbance was measured at 517 nm using a spectrophotometer (UV 1900, UV-VIS Spectrofotometer Shimadzu, USA, Manifacturing Inc., Canby Oregon, USA) employing methanol as a blank. All determinations were performed in triplicate. The radical scavenging ability of the tested compounds was calculated as follows:

Radical scavenging activity (%) = [(Ac—As)/Ac)] x 100.

where As represents the absorbance of the sample, and Ac is the absorbance of a DPPH solution as control. Because DMSO exhibits both pro-oxidant and antioxidant properties [46] its influence in the DPPH assay was investigated. Thus, various volumes of DMSO (10, 50, 100, 250, 500, 1000 μL) were made up to 1000 μL with MeOH. Then 1000 μL of DPPH solution were added, and the solutions were measured in triplicate, as mentioned above. The results (Table S3 and Fig. S5) showed that up to 1 mL DMSO can be used without affecting evaluation

of the free-radical scavenger activity of the compounds.

4.2.2. Data analysis

The percentage of inhibition of DPPH radical was determined, and the values were plotted into a graph showing the average inhibition of DPPH radical at the steady-state as a function of the molar concentration of tested compounds. The data were then analyzed using the GraphPad Prism statistical model described by Zheng et al. [47] and were expressed as EC_{50} values, defined as the concentration of antioxidant that produces a 50 % decrease in the DPPH concentration.

4.3. Chemical stability

4.3.1. Chemicals

Acetonitrile (Chromasolv), formic acid (MS grade), tris(hydroxymethyl)aminomethane hydrochloride (Tris HCl) were purchased by Sigma-Aldrich (Milan, Italy). Internal Standard (compound **15**, Scheme 2), Milli-Q water 18 MΩ was obtained from Millipore's Simplicity system (Milan-Italy). The 50 mM Tris buffer solution was prepared dissolving 0.8 g of tris(hydroxymethyl)aminomethane hydrochloride in 0.1 L of Milli-Q water.

4.3.2. Instrumental

The experiments were carried out with a Thermo Finnigan LCQ ion trap system equipped with Surveyor MS HPLC and an ESI source. Raw data was collected and processed by XCalibur 2.0. Thermostatic oven G-Therm 015 (F.lli Galli, Milan, Italy) was used to maintain the samples at 37 °C during the degradation test.

The HPLC-MS/MS parameters, the preparation of the calibration solutions, the linearity of the calibration curve, and the limit of detection of the quantitative method, for each studied compound, were reported in Supplementary Data.

4.4. Molecular modeling studies

4.4.1. Refinement of the human A_{2A}, A_1, and A_3 AR structures

The crystal structure of the hA_{2A} AR in complex with ZM241385, the crystal structure of hA_1 AR receptor in complex with PSB36, and the cryo-EM structure of hA_3 AR in complex with IB-MECA were retrieved from the Protein Data Bank (http://www.rcsb.org; pdb code: 5NM4, 1.7-Å resolution [38]; pdb code: 5N2S, 3.3-Å resolution [41]; pdb code: 8X16; 3.3-Å resolution [42], respectively). Since the three experimental structures present some residue mutations, the wild type sequence of each receptor was restored with the Homology Model tool of MOE (Molecular Operating Environment 2022.02) [39] and the structures were added of all hydrogen atoms within the same program.

4.4.2. Molecular docking analysis

All compound structures were docked into the binding site of the AR structures using the Induced Fit docking protocol of MOE [39] and the genetic algorithm docking tool of CCDC Gold [40]. The Induced Fit docking protocol of MOE is divided into a number of stages. *Conformational Analysis of ligands*. The algorithm generated conformations from a single 3D conformation by conducting a systematic search. In this way, all combinations of angles were created for each ligand. *Placement*. A collection of poses was generated from the pool of ligand conformations using Alpha Triangle placement method. *Scoring*. Poses generated by the placement methodology were scored using the *Alpha HB* scoring function, which combines a term measuring the geometric fit of the ligand to the binding site and a term measuring hydrogen bonding effects. *Induced Fit*. The generated docking conformations were subjected to energy minimization within the binding site and the protein side-chains are included in the refinement stage. *Rescoring*. Complexes generated by the Induced Fit methodology stage were scored using the *Alpha HB* scoring function. Gold tool was used with default efficiency settings, by selecting Chemscore, ASP, and PLP as scoring functions.

4.5. Pharmacology

4.5.1. Binding assay at ARs

Chinese hamster ovary (CHO) cells stably expressing human ARs were grown adherently and maintained in Dulbecco's Modified Eagles Medium with nutrient mixture F12 (DMEM/F12), supplemented with 10 % Fetal Bovine Serum (FBS), 100 U/mL penicillin, 100 μg/mL streptomycin, 2.5 μg/mL amphotericin, 1 mM sodium pyruvate, and 0.1 mg/mL Geneticin (G418) at 37 °C, and aerated with 5 % CO_2: 95 % O_2. Membrane preparations of recombinant CHO cells expressing the respective hARs were obtained as previously reported [48]. Radioligand binding assays for hA_1, hA_{2A}, and hA_3 ARs were performed using the following radioligands: [^{3}H]CCPA 1 nM for the hA_1 AR, [^{3}H]NECA 10 nM for hA_{2A} AR, and [^{3}H]HEMADO 1 nM for the hA_3 AR. Three-five separate experiments were performed for determination of K_i values which are given as the mean ± standard error (S.E.). The potency of antagonists at the hA_{2B} AR (expressed on CHO cells) was determined by inhibition of NECA-stimulated adenylyl cyclase activity.

All data were analyzed with GraphPad Prism (GraphPad Software, San Diego, CA, USA).

4.5.2. cAMP assay

Functional activity was determined as described earlier [48]. Briefly, CHO cells stably expressing either the hA_{2A} AR or hA_{2B} AR and the plasmid pGloSensor-22F coding for the biosensor were incubated for 2 h with the GloSensor cAMP reagent. Cells were subsequently dispensed in the wells of a 384-well plate and the reference agonist NECA or the under-study compounds were added at different concentrations. Since the ability of compounds to stimulate (A_{2A} and A_{2B} ARs) the cAMP production did not produce results, the antagonist profile was evaluated by assessing the ability to counteract an NECA-induced increase in cAMP accumulation. Responses were expressed as a percentage of the maximal relative luminescence units (RLU). Concentration–response curves were fitted by a nonlinear regression using Prism software. Each concentration was tested three-five times in duplicate and the values are given as the mean ± standard error (S.E.).The antagonist profile of the compounds was expressed as the $IC_{50,}$ which is the concentration of antagonist that produces a 50 % inhibition of the agonist effect.

4.5.3. In vitro models of cerebral ischemia

4.5.3.1. Animals and ethical approval. Male Wistar rats (150–180 g body weight, 6–8 weeks old), used for extracellular recordings, were purchased from Envigo (Udine, Italy). Male and female Wistar rat pups (7–9 days old), used for organotypic cultures, were purchased from Charles River (Milan, MI, Italy). All experimental procedures were carried out following the Italian regulations for the care and use of laboratory animals (EU Directive 2010/63/EU) and were approved by appropriate institutional and state authorities of the University of Florence (301/2021 for acute slices; 17E9C.N.GS0. for organotypic slices). In compliance to Italian law and EU directives, all efforts were made to minimize the number of animals used and suffering according to the principle of 3Rs. All animals were located in a temperature-controlled room (22 ± 1 °C), with food and water ad libitum, and with a 12 h light/dark cycle.

4.5.3.2. Drugs. Both for extracellular recordings and for organotypic slice experiments all drugs were dissolved in dimethyl sulphoxide (DMSO). Stock solutions, of 1000–10,000 times the desired final concentration, were stored at −20 °C. The final concentration of DMSO (0.1 % in aCSF) used in our experiments did not alter electrophysiological properties or drugs effects in hippocampal slices.

4.5.3.3. Preparation of acutely isolated hippocampal slices. Acute hippocampal slices were prepared as previously described [49]. Animals were sacrificed via decapitation under anesthesia with isoflurane (Baxter,

Rome, Italy). The hippocampi were rapidly dissected and transferred in ice-cold oxygenated (95 % O_2–5 % CO_2) artificial cerebrospinal fluid (aCSF) of the following composition (mM): NaCl 125, KCl 3, NaH_2PO_4 1.25, $MgSO_4$ 1, $CaCl_2$ 2, $NaHCO_3$ 25, and D-glucose 10. Slices (400 μM nominal thickness) were cut using a McIlwain Tissue Chopper (Mickle Laboratory Engineering Co. Ltd., Gomshall, United Kingdom) and kept in oxygenated aCSF for at least 1 h at room temperature. During recordings, each slice was placed on a nylon mesh, fully submerged in a small-volume chamber (0.8 mL), and superfused with oxygenated aCSF maintained at 31–32 °C at a steady flow rate of 2 mL/min. The perfused solutions reached the preparation in 60 s and this delay was considered in our calculations.

4.5.3.3.1. Extracellular recordings and oxygen-glucose deprivation. Test pulses (80 μs, 0.066 Hz) were applied through a bipolar nichrome electrode located in the stratum radiatum of the CA1 region of rat hippocampal slices to stimulate the Schaffer collateral-commissural fibers. Extracellular potentials were recorded using borosilicate microelectrodes (2–10 MΩ, Harvard Apparatus LTD, United Kingdom) filled with 150 mM NaCl. The recording electrode was positioned in the apical dendritic layer of CA1 region to record field excitatory postsynaptic potentials (fEPSPs). Data were amplified (200×, BM 622, Mangoni, Pisa, Italy), digitized (sample rate, 33.33 kHz), and stored for later analysis with LTP (version 2.30D) program [50]. Once a stable baseline of evoked responses was established, fEPSP amplitudes were routinely measured and expressed as the percentage of the mean value recorded 2 min before the application of any pharmacological treatment (pre-OGD). The test stimulus intensity was then adjusted to generate a synaptic response of about 40 % of the maximum and was held constant throughout the experiment. Simultaneously, AD was recorded as negative extracellular direct current (d.c.) shifts induced by OGD. The d.c. potential reflects the membrane polarization of cells surrounding the recording electrode tip [51]. AD latency, expressed in min, was calculated from the beginning of OGD; AD amplitude, expressed in mV, was measured at the maximal negativity peak and it was expressed as positive values in the text and bar graphs. Oxygen-glucose deprivation (OGD) was obtained by superfusing the slice with glucose-free aCSF, gassed with nitrogen (95 % N_2–5 % CO_2) [49] for 30 min. This OGD-time duration does not permit the recovery of fEPSPs causing irreversible synaptic failure, as previously described [45]. Each compound tested was applied 15 min before, during, and 5 min after OGD.

4.5.3.4. Rat organotypic hippocampal slices exposed to oxygen-glucose deprivation. Male and female Wistar rat pups were purchased from Charles River (MI, Italy). Organotypic hippocampal slice cultures were prepared as previously described [52]. Briefly, the hippocampi were removed from the brains of 7–9 day old Wistar rats and transverse slices (420 μm) were prepared using a McIlwain tissue chopper in a sterile environment. Isolated slices were first placed in ice-cold Hanks' balanced salt solution (HBSS), supplemented with 5 mg/mL glucose and 1.5 % Fungizone® (GIBCO-BRL), then transferred to humidified semi-porous membranes (30 mm Millicell-CM 0.4 μm tissue culture plate inserts, Millipore, Italy; 4 per membrane). These were placed in six-well tissue culture plates containing 1.2 mL culture medium containing 50 % Eagle's MEM, 25 % heat-inactivated horse serum, 25 % HBSS, 5 mg/mL glucose, 1 mM glutamine and 1.5 % Fungizone®. Slices were maintained at 37 °C, with 100 % humidity, and 95 % air/5 % CO_2 atmosphere and the medium was changed every three days. Experiments were carried out after 14 days in vitro (DIV). Oxygen and glucose deprivation (OGD) was induced as previously described [40]. Briefly, the slices were exposed to a serum-free medium saturated with 95 % N_2/5 % CO_2 at 37 °C in a gassed incubator equipped with an oxygen controller (BioSpherix, New York, USA). After 30 min, the cultures were transferred to oxygenated serum-free medium containing 5 mg/mL glucose and returned to the incubator under normoxic conditions. Drugs were incubated during 30 min OGD and in subsequent 24 h. Cell injury was evaluated 24 h later and was assessed using the fluorescent dye propidium iodide (PI) (5 μg/mL) that was added to the medium at the end of the 24 h recovery period. Fluorescence was viewed using an inverted fluorescence microscope (Olympus IX-50; Solent Scientific, Segensworth, UK) equipped with a xenon-arc lamp, a low-power objective (4×) and a rhodamine filter. Images were digitized using a video image obtained with a CCD camera (Diagnostic Instruments Inc., Sterling Heights, MI, USA) controlled by software (InCyt Im1TM; Intracellular Imaging Inc., Cincinnati, OH, USA) and subsequently analyzed using the Image-Pro Plus morphometric analysis software (Media Cybernetics, Silver Spring, MD, USA). To quantify cell damage, the CA1 hippocampal subfield was identified and encompassed in a frame using the drawing function in the image software (ImageJ; NIH, Bethesda, MD, USA) and the optical density of PI fluorescence was recorded.

4.5.3.5. Statistical analysis. Data were expressed as mean ± SD. The statistical significance of differences between control and treatment groups in electrophysiology data and PI fluorescence intensities was analyzed using one-way ANOVA with a post hoc Tukey-test for multiple comparisons. Data were analyzed using "GraphPad Prism v.8" (GraphPad Software, San Diego, CA, USA) software. A probability value (p) of <0.05 was considered significant.

CRediT authorship contribution statement

Sara Calenda: Methodology, Investigation, Formal analysis. **Costanza Ceni:** Methodology, Investigation. **Daniela Catarzi:** Writing – review & editing, Formal analysis. **Flavia Varano:** Writing – review & editing, Formal analysis. **Giulia Vagnoni:** Investigation. **Gian luca Bartolucci:** Methodology, Formal analysis, Data curation. **Marta Menicatti:** Methodology, Investigation, Data curation. **Gabriella Marucci:** Methodology, Data curation. **Michela Buccioni:** Methodology, Investigation, Formal analysis. **Diego Dal Ben:** Writing – original draft, Methodology, Investigation, Formal analysis, Data curation. **Rosaria Volpini:** Writing – review & editing, Formal analysis. **Antonella Capperucci:** Formal analysis, Data curation. **Damiano Tanini:** Methodology, Investigation, Data curation. **Martina Venturini:** Methodology, Investigation, Data curation. **Elisa Landucci:** Writing – original draft, Methodology, Investigation, Formal analysis, Data curation. **Clara Santalmasi:** Investigation. **Federica Cherchi:** Investigation. **Costanza Mazzantini:** Investigation. **Anna Maria Pugliese:** Writing – original draft, Methodology, Funding acquisition, Formal analysis, Data curation, Conceptualization. **Domenico E. Pellegrini-Giampietro:** Writing – review & editing, Funding acquisition, Conceptualization. **Vittoria Colotta:** Writing – review & editing, Writing – original draft, Supervision, Funding acquisition, Conceptualization.

Declaration of competing interest

The authors declare that they have no known competing financial interests or personal relationships that could have appeared to influence the work reported in this paper.

Acknowledgments

The work was funded by NEXT-GENERATION-EU (NGEU)-National Recovery and Resilience Plan (NRRP), Mission 4 - Component 2. Investment 1.5-Ministry of University and Research (MUR) Call n° 3277, Project Code ECS_00000017 – MUR Directoral Decree no.1055, 23 June 2022, CUP B83C22003920001. Project title" Tuscany Health Ecosystem-THE, Spoke 8 (S.C.; D.C.; V.C.; F.V.) - NEXT-GENERATION-EU (NGEU)-National Recovery and Resilience Plan (NRRP), project MNESYS (PE0000006) (DR. 1553 11.10.2022) (D.E.P.G.)

-NEXT-GENERATION-EU (NGEU)-National Recovery and Resilience Plan (NRRP), M4C2 Investment 1.4 [CN00000041 CN3 "National Center

for Gene Therapy and Drugs based on RNA Technology" Spoke 3 CUP: B13C22001010001] (A.M.P.; E.L.).

Appendix A. Supplementary data

Supplementary data to this article can be found online at https://doi.org/10.1016/j.bioorg.2025.108855.

Data availability

No data was used for the research described in the article.

References

[1] P.A. Borea, S. Gessi, S. Merighi, F. Vincenzi, K. Varani, Pharmacology of adenosine receptors: the state of the art, Physiol. Rev. 98 (2018) 1591–1625.

[2] F. Vincenzi, S. Pasquini, C. Contri, M. Cappello, M. Nigro, A. Travagli, S. Merighi, S. Gessi, P.A. Borea, K. Varani, Pharmacology of adenosine receptors: recent advancements, Biomolecules 13 (2023) 1387.

[3] S.A. Rivkees, S. Thevananther, H. Hao, Are A_3 adenosine receptors expressed in the brain? NeuroReport 11 (2000) 1025–1030.

[4] M.-F. Ho, L.M. Low, R.B. Meyer, Pharmacology of the adenosine A_3 receptor in the vasculature and essential hypertension, PLoS One 11 (2016) e0150021.

[5] J. Stockwell, E. Jakova, F. Cayabyab, Adenosine A_1 and A_{2A} receptors in the brain: current research and their role in neurodegeneration, Molecules 22 (2017) 676.

[6] Y. Zhang, B. Wernly, X. Cao, S.J. Mustafa, Y. Tang, Z. Zhou, Adenosine and adenosine receptor-mediated action in coronary microcirculation, Basic Res. Cardiol. 116 (2021) 22.

[7] M. Lovászi, Z.H. Németh, P. Pacher, W.C. Gause, G. Wagener, G. Haskó, A_{2A} adenosine receptor activation prevents neutrophil aging and promotes polarization from N1 towards N2 phenotype, Purinergic Signal 18 (2022) 345–358.

[8] I. Dettori, L. Gaviano, F. Ugolini, D. Lana, I. Bulli, G. Magni, F. Rossi, M. G. Giovannini, F. Pedata, Protective effect of adenosine A_{2B} receptor agonist, BAY60-6583, against transient focal brain ischemia in rat, Front. Pharmacol. 11 (2021) 588757.

[9] Y.-J. Liu, J. Chen, X. Li, X. Zhou, Y.-M. Hu, S.-F. Chu, Y. Peng, N.-H. Chen, Research progress on adenosine in central nervous system diseases, CNS Neurosci. Ther. 25 (2019) 899–910.

[10] F. Pedata, A.M. Pugliese, E. Coppi, I. Dettori, G. Maraula, L. Cellai, A. Melani, Adenosine A_{2A} receptors modulate acute injury and neuroinflammation in brain ischemia, Mediat. Inflamm. (2014) (Article ID 805198, 16 pages).

[11] Y. Zhou, X. Zeng, G. Li, Q. Yang, J. Xu, M. Zhang, X. Mao, Y. Cao, L. Wang, Y. Xu, Y. Wang, Y. Zhang, Z. Xu, C. Wu, J.-F. Chen, M.N. Hoda, Z. Liu, M. Hong, Y. Huo, Inactivation of endothelial adenosine A_{2A} receptors protects mice from cerebral ischaemia-induced brain injury, Br. J. Pharmacol. 176 (2019) 2250–2263.

[12] R.A. Mohamed, A.M. Agha, A.A. Abdel-Rahman, N.N. Nassar, Role of adenosine A_{2A} receptor in cerebral ischemia-reperfusion injury: signaling to phosphorylated extracellular signal-regulated protein kinase (pERK1/2), Neuroscience 314 (2016) 145–159.

[13] N. Revi Jiang, T. Yang, H. Han, J. Shui, M. Hou, W. Wei, G. Kumar, L. Song, C. Ma, Z. Li, Ding exploring Research Trend and hotspots on oxidative stress in ischemic stroke (2001−2022): insights from bibliometric, Mol. Neurobiol. 61 (2024) 6200–6216.

[14] J.J. Lochhead, P.T. Ronaldson, T.P. Davis, The role of oxidative stress in blood–brain barrier disruption during ischemic stroke: antioxidants in clinical trials, Biochem. Pharmacol. 228 (2024) 116186.

[15] Z. Song, L. Ye, Y. Wang, W. Wang, C. Liu, J. Lu, J. Zhang, H. Wang, J. Zhang, Y. Yang, J. Tian, Targeting RIPK1-mediated necroptosis, oxidative stress, and ferroptosis: a novel multitarget therapy for ischemic stroke, Eur. J. Med. Chem. 296 (2025) 117884.

[16] Y. Fu, A. Wang, R. Tang, S. Li, X. Tian, X. Xia, J. Ren, S. Yang, R. Chen, S. Zhu, X. Feng, J. Yao, Y. Wei, X. Dong, Y. Ling, F. Yi, Q. Deng, C. Guo, Y. Sui, S. Han, D. Fan, Sublingual Edaravone Dexborneol for the treatment of acute ischemic stroke: the TASTE-SL randomized clinical trial, JAMA Neurol. 81 (2024) 319–326.

[17] M. Falsini, D. Catarzi, F. Varano, D. Dal Ben, G. Marucci, M. Buccioni, R. Volpini, L. Di Cesare Mannelli, E. Lucarini, C. Ghelardini, G. Bartolucci, M. Menicatti, V. Colotta, Antioxidant-conjugated 1,2,4-triazolo[4,3-a]pyrazin-3-one derivatives: highly potent and selective human A_{2A} adenosine receptor antagonists possessing protective efficacy in neuropathic pain, J. Med. Chem. 62 (62) (2019) 8511–8531.

[18] T. Yamashita, K. Abe, Update on antioxidant therapy with Edaravone: expanding applications in neurodegenerative diseases, Int. J. Mol. Sci. 25 (2024) 2945.

[19] Z. Shakkour, H. Issa, H. Ismail, O. Ashekyan, K.J. Habashy, L. Nasrallah, H. Jourdi, E. Hamade, S. Mondello, M. Sabra, K. Zibara, F. Kobeissy, Drug repurposing: promises of Edaravone target drug in traumatic brain injury, Curr. Med. Chem. 28 (2021) 2369–2391.

[20] N. Zhang, M. Komine-Kobayashi, R. Tanaka, M. Liu, Y. Mizuno, T. Urabe, Edaravone reduces early accumulation of oxidative products and sequential inflammatory responses after transient focal ischemia in mice brain, Stroke 36 (2005) 2220–2225.

[21] J. Liu, Y. Jiang, G. Zhang, Z. Lin, S. Du, Protective effect of edaravone on blood-brain barrier by affecting NRF-2/HO-1 signaling pathway, Exp. Ther. Med. 18 (2019) 2437–2442.

[22] G. Jin, W. Han, T. Duan, Z. Xue, C. Song, Y. Xu, M. Yu, Edaravone dextranol alleviates ferroptosis, cuproptosis, and blood-brain barrier damage after acute cerebral infarction, Metab. Brain Dis. 40 (2025) 134.

[23] P. Porta, S. Aebi, K. Summer, B.H. Lauterburg, L-2-Oxothiazolidine-4-carboxylic acid, a cysteine prodrug: pharmacokinetics and effects on thiols in plasma and lymphocytes in human, J. Pharmacol. Exp. Ther. 257 (1991) 331–334.

[24] S.J. Park, K.S. Lee, S.J. Lee, S.R. Kim, S.Y. Park, M.S. Jeon, H.B. Lee, Y.C. Lee, L-2-Oxothiazolidine-4-carboxylic acid or α-lipoic acid attenuates airway remodeling: involvement of nuclear factor-kB (NF-kB), nuclear factor erythroid 2p45-related factor-2 (Nrf2), and hypoxia-inducible factor (HIF), Int. J. Mol. Sci. 13 (2012) 7915–7937.

[25] W. Promsote, R. Veeranan-Karmegam, S. Ananth, D. Shen, C.-C. Chan, N. A. Lambert, V. Ganapathy, P.M. Martin, *L*-2-oxothiazolidine-4-carboxylic acid attenuates oxidative stress and inflammation in retinal pigment epithelium, Mol. Vis. 20 (2014) 73–88.

[26] Y. Liu, J.-W. Min, S. Feng, K. Subedi, F. Qiao, E. Mammenga, E. Callegari, H. Wang, Therapeutic role of a cysteine precursor, OTC, in ischemic stroke is mediated by improved proteostasis in mice, Transl. Stroke Res. 11 (2020) 147–160.

[27] G. Ni, Z. Hu, Z. Wang, M. Zhang, X. Liu, G. Yang, Z. Yan, Y. Zhang, Cysteine donor-based brain-targeting prodrug: opportunities and challenges oxidative, Oxidative Med. Cell. Longev. 4834117 (2022) 16.

[28] S.Y. Park, K.Y. Kim, D.S. Gwak, S.Y. Shin, D.Y. Jun, Y.H. Kim, L-cysteine mitigates ROS-induced apoptosis and neurocognitive deficits by protecting against endoplasmic reticulum stress and mitochondrial dysfunction in mouse neuronal cells, Biomed. Pharmacother. 180 (2024) 117538.

[29] M. Falsini, D. Catarzi, F. Varano, D. Dal Ben, G. Marucci, M. Buccioni, R. Volpini, L. Di Cesare Mannelli, C. Ghelardini, V. Colotta, Novel 8-amino-1,2,4-triazolo[4,3-a]pyrazin-3-one derivatives as potent human adenosine A_1 and A_{2A} receptor antagonists. Evaluation of their protective effect against β-amyloid-induced neurotoxicity in SH-SY5Y cells, Bioorg. Chem. 87 (2019) 380–394.

[30] P. Wang, Y. Cheng, C. Wu, Y. Zhou, Z. Cheng, H. Li, R. Wang, W. Su, L. Fang, Tyrosine-specific modification via a dearomatization-rearomatization strategy: access to azobenzene functionalized peptides, Org. Lett. 23 (2021) 4137–4141.

[31] M. Falsini, C. Ceni, D. Catarzi, F. Varano, D. Dal Ben, G. Marucci, M. Buccioni, A. Marti Navia, R. Volpini, V. Colotta, New 8-amino-1,2,4-triazolo[4,3-a]pyrazin-3-one derivatives. Evaluation of different moieties on the 6-aryl ring to obtain potent and selective human A_{2A} adenosine receptor antagonists, Bioorg. Med. Chem. Lett. 30 (2020) 127126.

[32] K. Chegaev, C. Cena, M. Giorgis, B. Rolando, P. Tosco, M. Bertinaria, R. Fruttero, P.-A. Carrupt, A. Gasco, Edaravone derivatives containing NO-donor functions, J. Med. Chem. 52 (2009) 574–578.

[33] J. DeRuiter, D.A. Carter, W.S. Arkledge, P.J. Sullivan, Synthesis and reaction of 4-isopropylidene-1-aryl-3-methyl-2-pyrazolin-5-ones, J. Heterocyclic Chem. 24 (1987) 149–153.

[34] H. Maruoka, K. Yamagata, F. Okabe, Y. Tomioka, Synthesis of acyl-1,2-dihydro-3H-pyrazol-3-ones via Lewis acid-mediated rearrangement of 3-acyloxypyrazoles, J. Heterocyclic Chem. 43 (2006) 859–865.

[35] M. Seki, M. Hatsuda, Y. Mori, S.-I. Yoshida, S.-I. Yamada, T. Shimizu, A practical synthesis of (+) biotin from L-cysteine, Chem. Eur. J. 10 (2004) 6102–6110.

[36] P. Sricharoen, S. Techawongstein, S. Chanthai, A high correlation indicating for an evaluation of antioxidant activity and total phenolics content of various chilli varieties, J. Food Sci. Technol. 52 (2015) 8077–8085.

[37] F. Dholkawala, C. Voshavar, A.K. Dutta, Synthesis and characterization of brain penetrant prodrug of neuroprotective D-264: potential therapeutic application in the treatment of Parkinson's disease, Eur. J. Pharm. Biopharm. 103 (2016) 62–70.

[38] T. Weinert, N. Olieric, R. Cheng, S. Brunle, D. James, D. Ozerov, D. Gashi, L. Vera, M. Marsh, K. Jaeger, F. Dworkowski, E. Panepucci, S. Basu, P. Skopintsev, A. S. Dore, T. Geng, R.M. Cooke, M. Liang, A.E. Prota, V. Panneels, P. Nogly, U. Ermler, G. Schertler, M. Hennig, M.O. Steinmetz, M. Wang, J. Standfuss, Serial millisecond crystallography for routine room-temperature structure determination at synchrotrons, Nat. Commun. 8 (2017) 542.

[39] Molecular Operating Environment, C.C.G., Inc., 1255 University St., Suite 1600, Montreal, Quebec, Canada, H3B 3X3, 2025.

[40] G. Jones, P. Willett, R.C. Glen, A.R. Leach, R. Taylor, Development and validation of a genetic algorithm for flexible docking, J. Mol. Biol. 267 (1997) 727–748.

[41] R.K.Y. Cheng, E. Segala, N. Robertson, F. Deflorian, A.S. Dore, J.C. Errey, C. Fiez-Vandal, F.H. Marshall, R.M. Cooke, Structures of human A_1 and A_{2A} adenosine receptors with xanthines reveal determinants of selectivity, Structure 25 (2017) 1275–1285 e1274.

[42] H. Cai, S. Guo, Y. Xu, J. Sun, J. Li, Z. Xia, Y. Jiang, X. Xie, H.E. Xu, Cryo-EM structures of adenosine receptor A_3 AR bound to selective agonists, Nat. Commun. 15 (2024) 3252.

[43] C. Mazzantini, M. Venturini, D. Lana, G. Mulas, C. Santalmasi, G. Magni, P. Bruni, A.M. Pugliese, F. Cencetti, D.E. Pellegrini-Giampietro, E. Landucci, Dual action of sphingosine 1-phosphate pathway in in vitro models of global cerebral ischemia, Neurobiol. Dis. 208 (2025) 106865.

[44] A.M. Pugliese, E. Coppi, G. Spalluto, R. Corradetti, F. Pedata, A_3 adenosine receptor antagonists delay irreversible synaptic failure caused by oxygen and glucose deprivation in the rat CA1 hippocampus in vitro, Br. J. Pharmacol. 147 (2006) 524–532.

[45] A.M. Pugliese, C. Traini, S. Cipriani, M. Gianfriddo, T. Mello, M.G. Giovannini, A. Galli, F. Pedata, The adenosine A_{2A} receptor antagonist ZM241385 enhances neuronal survival after oxygen-glucose deprivation in rat CA1 hippocampal slices, Br. J. Pharmacol. 157 (157) (2009) 818–830.

[46] C. Sanmartín-Suárez, R. Soto-Otero, I. Sanchez-Sellero, E. Mendez-Alvarez, Antioxidant properties of dimethyl sulfoxide and its viability as a solvent in the

evaluation of neuroprotective antioxidants, J. Pharmacol. Toxicol. Methods 63 (2011) 209–215.
[47] C. Zheng, R. Bertin, G. Froldi, EC_{50} estimation of antioxidant activity in DPPH assay using several statistical programs, Food Chem. 138 (2013) 414–420.
[48] A. Spinaci, M. Buccioni, D. Catarzi, C. Cui, V. Colotta, D. Dal Ben, E. Cescon, B. Francucci, I. Grieco, C. Lambertucci, G. Marucci, D. Bassani, M. Pavan, F. Varano, S. Federico, G. Spalluto, S. Moro, R. Volpini, Dual anta-inhibitors of the A_{2A} adenosine receptor and casein kinase CK1delta: synthesis, biological evaluation, and molecular modeling studies, Pharmaceuticals 16 (2023) 167.
[49] M. Venturini, F. Cherchi, C. Santalmasi, L. Frulloni, I. Dettori, D. Catarzi, F. Pedata, V. Colotta, F. Varano, E. Coppi, A.M. Pugliese, Pharmacological characterization of P626, a novel dual adenosine A_{2A}/A_{2B} receptor antagonist, on synaptic plasticity and during an ischemic-like insult in CA1 rat hippocampus, Biomolecules 13 (2023) 894.
[50] W.W. Anderson, G.L. Collingridge, The LTP program: a data acquisition program for on-line analysis of long-term potentiation and other synaptic events, J. Neurosci. Methods 108 (2001) 71–83.
[51] E. Farkas, R. Pratt, F. Sengpiel, T.P. Obrenovitch, Direct, live imaging of cortical spreading depression and anoxic depolarization using a fluorescent, voltage-sensitive dye, J. Cereb. Blood Flow Metab. 28 (2007) 251–262.
[52] E. Landucci, R. Berlinguer-Palmini, G. Baccini, F. Boscia, E. Gerace, G. Mannaioni, D.E. Pellegrini-Giampietro, The neuroprotective effects of mGlu1 receptor antagonists are mediated by an enhancement of GABAergics transmission via a presynaptic CB1 receptor mechanism, Cells 11 (2022) 3015.